Performance Analysis of a UMTS-based Passive Multistatic Radar operating in a Line-of-Sight Environment

By

Muhammad Nohman Javed

NUST201362832MSEECS61213F

Supervisor

Dr. Syed Ali Hassan

Department of Electrical Engineering

A thesis submitted in partial fulfillment of the requirements for the degree of Masters in Electrical Engineering (MS EE-TCN)

In

School of Electrical Engineering and Computer Science,

National University of Sciences and Technology (NUST),

Islamabad, Pakistan.

(Dec, 2015)

Approval

It is certified that the contents and form of the thesis entitled " **Performance Analysis of a UMTS-based Passive Multistatic Radar operating in a Line-of-Sight Environment**" submitted by **Muhammad Nohman Javed** have been found satisfactory for the requirement of the degree.

Advisor: **Dr. Syed Ali Hassan**

Signature: _____

Date: _____

Committee Member 1: **Dr. Sajid Saleem**

Signature: _____

Date: _____

Committee Member 2: **Dr. Sajid Ali**

Signature: _____

Date: _____

Committee Member 3: **Dr. Fahd Ahmed Khan**

Signature: _____

Date: _____

Dedication

I dedicate this dissertation to my parents, my brothers, sister and all those who support me throughout this journey of my dissertation research.

Certificate of Originality

I hereby declare that this submission is my own work and to the best of my knowledge it contains no materials previously published or written by another person, nor material which to a substantial extent has been accepted for the award of any degree or diploma at NUST SEECS or at any other educational institute, except where due acknowledgement has been made in the thesis. Any contribution made to the research by others, with whom I have worked at NUST SEECS or elsewhere, is explicitly acknowledged in the thesis.

I also declare that the intellectual content of this thesis is the product of my own work, except for the assistance from others in the project's design and conception or in style, presentation and linguistics which has been acknowledged.

Author Name: **Muhammad Nohman Javed**

Signature: _____

Acknowledgment

First of all, I am very thankful to Allah (S.W.T) who enable me and make all of tasks easy for me. I am very thankful to my parents, brothers, sister, relatives and friends who pray for me and support me throughout this phase.

I am very grateful to my supervisor Dr. Syed Ali Hassan for his consistent support, encouragement, valuable suggestion and guidance. I am also thankful to him for galvanizing my morale in difficult times.

I am indebted to my committee member Dr. Sajid Ali for building my mathematical skills. Finally, I am also thankful to other committee members Dr. Fahd Ahmed Khan and Dr. Sajid Saleem for giving me their valuable time and guidance. **Muhammad Nohman Javed**

Table of Contents

1 Introduction **1**

1.1 Passive Radar 1

1.2 History of Passive Radar 1

1.3 Advantages of Passive Radar 2

1.4 Disadvantages of Passive Radar 3

1.5 Applications of Passive Radar 3

1.6 Bistatic Geometry 4

1.7 Literature Review 5

1.7.1 UMTS Signal and Related work 6

1.8 Problem formulation and its significance 8

1.9 Contributions 11

1.10 Thesis Organization 11

2 Signal Model **12**

3 Derivation of MCRLB **18**

4 Numerical Results **28**

5 Concluding Remarks **39**

Appendices **41**

A Proof of Theorem 1 **42**

A.1 Entries of MFIM 57

A.2 Proof of Lemma 2 59

List of Figures

1.1 North referenced Bistatic Geometry. 4

2.1 Impulse response of an RRC pulse for different values of α. . . 14

4.1 Simulated multistatic 3D scenarios 1 and 2 with positions of transmitters $\mathbf{T}_i$, receivers $\mathbf{R}_j$ and target $\mathbb{T}$. 29

4.2 RMCRLB variation with κ for x-component of target position $[3.4, 2.5, 3.7]$ (Km). 29

4.3 RMCRLB variation with κ for y-component of target position $[3.4, 2.5, 3.7]$ (Km). 30

4.4 RMCRLB variation with κ for z-component of target position $[3.4, 2.5, 3.7]$ (Km). 30

4.5 RMCRLB variation with κ for x-component of target velocity $[30, 20, 25]$ (m/sec). 31

4.6 RMCRLB variation with κ for y-component of target velocity $[30, 20, 25]$ (m/sec). 32

4.7 RMCRLB variation with κ for z-component of target velocity $[30, 20, 25]$ (m/sec). 32

4.8 Transceiver pairs with and without LoS component. 33

4.9 RMCRLB vs Υ_{NLoS} for x-component of target position $[3.5, 4.5, 2.1]$ (Km) with various transceiver pairs selection for LoS. 34

4.10 RMCRLB vs Υ_{NLoS} for y-component of target position $[3.5, 4.5, 2.1]$ (Km) with various transceiver pairs selection for LoS. 34

4.11 RMCRLB vs Υ_{NLoS} for z-component of target position $[3.5, 4.5, 2.1]$ (Km) with various transceiver pairs selection for LoS. 35

4.12 RMCRLB vs Υ_{NLoS} for x-component of target velocity $[35, 45, 15]$ (m/sec) with various transceiver pairs selection for LoS. . . . 36

4.13 RMCRLB vs Υ_{NLoS} for y-component of target velocity $[35, 45, 15]$ (m/sec) with various transceiver pairs selection for LoS. . . . 36

4.14 RMCRLB vs Υ_{NLoS} for z-component of target velocity $[35, 45, 15]$ (m/sec) with various transceiver pairs selection for LoS. . . . 37

4.15 RMCRLB vs observation time for target position $[3.5, 4.5, 2.1]$ (Km). 38

List of Tables

4.1 Transmitters and Receivers positions (Km) 28

List of Abbreviations

Abbreviation	Description
UMTS	universal mobile telecommunication system
LoS	line-of-sight
MCRLB	modified Cramer-Rao lower bound
GRCSM	generalized radar cross section model
DAB	digital audio broadcast
DVB	digital video broadcast
GSM	global system for mobile communication
LTE	long term evolution
WIMAX	worldwide interoperability for microwave access
WRAN	wireless regional area network
FDD	frequency division duplexing
TDD	time division duplexing
QPSK	Quadrature phase shift keying
MIMO	multi input multi output

Abstract

In this work, the performance of a universal mobile telecommunication system (UMTS)-based passive multistatic radar in a line-of-sight (LoS) environment is studied. The presence of LoS component considerably alters the received signal model, therefore, its characterization is necessary and is the main subject of this work where the transceivers and a target are localized in two- dimensional and three-dimensional Euclidean spaces. The probability density function (PDF) of the received signal in the presence of LoS is derived and the closed-form expressions of the modified Cramer-Rao lower bounds (MCRLBs) on the Euclidean coordinates of target's position and velocity are found. It is shown that the modified Fisher information matrix (MFIM) is a combination of MFIM due to non-LoS (NLoS) components and LoS component. With the aid of numerical examples, it is verified that by exploiting LoS, the target radar cross section (RCS) increases, which improves the accuracy of target's detection and parameter estimation. In addition, it is also shown that by using a LoS geometry, the performance limits of a waveform can be determined for a generalized radar cross section model (GRCSM), which provides the characterization of a waveform for a broader range of radar applications.

Chapter 1

Introduction

1.1 Passive Radar

Passive radar is a type of bistatic radar which do not use its own dedicated transmitter to emit electromagnetic radiations. It utilizes the signals readily available in the environment from other illuminator of opportunities such as broadcast and telecommunication sources. In literature, passive radar is also called as Passive Coherent Location (PCL) and Passive Bistatic Radar. When more than one receiver or transmitter are used the passive radar is known as passive multistatic radar.

1.2 History of Passive Radar

The idea of passive radar is not new. Infact, the very earliest radar were bistatic and passive. The first passive radar 'Klein Heidelberg' was developed by Germans in 1943 [1]. The receivers were deployed along the cost lines to

use British Chain home radar as opportunity illuminators. However, with the development of duplexers(T_x/R_x switches) and pulse waveforms it is possible to transmit and receive the signal with the same antenna. Thus, making the active radar design both cost saving and space saving [2, 3]. But with the emergence and rapid growth of wireless technologies from short range 802.11 to long range cellular,audio and video broadcast technologies result in abundant availability of these RF signals in the environment. This trend results in upsurge the interest of people both in academia and industry to exploit the numerous advantages of passive radars by making use of these technologies.

1.3 Advantages of Passive Radar

- The very first advantage is it eliminates the need of dedicated transmitter hardware circuitry and allocation of dedicated RF band for signal tranmission. Thus, cut down the cost corresponding to installation, maintenace, operation and RF band allocation.

- No emission of RF energy from dedicated transmitter in passive radar is invulnerable to cause RF pollution. Thus, making passive radar an environment friendly technology.

- In passive radar usually phased array antennas are used which makes it more reliable than conventional radar as no movement of mechanical parts are required.

- When use in multistatic configuration, it provides the spatial and fre-

quency diversity which serve to improve the accuracy of target detection and estimation of its parameters.

- The same reason make it potential technology for stealth detection, antijamming [4] and many other advantages briefly discussed in [5] and explained in references therein.

1.4 Disadvantages of Passive Radar

- The passive radar has more complicated geometry, system complexity and excessive computation.
- The transmitted signals are not designed for radar operation purposes and are not in control.
- The technology is not mature enough.

1.5 Applications of Passive Radar

Passive Radars has potential applications in the following areas:

- Used in wi-see (through the wall sensing) a technology that will be added in mobiles to see behind the walls [6].
- Used in Detection of Low Probability of Intercept (LPI) Radar signals.
- Also used in detection of Stealth Targets.
- It is also used in Low Cost Air Traffic Control (ATC) Systems.

- Used in Law Enforcement such as Traffic Monitoring.
- Used in Border Crossing/Intrusion Detection.
- It can also be used in Local Metrological Monitoring.
- In astronomy it can be used for Planetary Mapping.
- It is used in synthetic aperture radar (SAR) imaging and its applications.

1.6 Bistatic Geometry

In this dissertation our focus is to determine the Modified Cramer Rao Lower Bound (MCRLB) on target parameters (position and velocity) by exploiting UMTS signals. For this, it is important to understand the bistatic geometry .

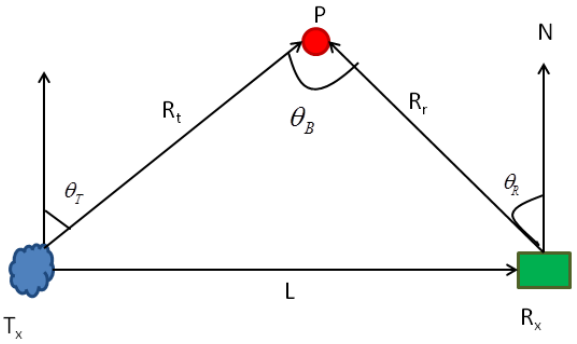

Figure 1.1: North referenced Bistatic Geometry.

In bistatic geometry, the transmitter T_x, receiver R_x and target P are represented by vertices of a triangle known as bistatic triangle as shown in the Fig. 1.1. The sides of this triangle R_t, R_r and L represent the range from transmitter to target, the range from receiver to target and the baseline between transmitter and receiver respectively. The angle θ_B formed between the transmitting path and echo path at the vertex representing target is called bistatic angle. For bistatic geometry, this angel θ_B is between $20^o < \theta_B < 145^o$. For monostaic geometry the angle $\theta_B < 45^o$ and for the forward fence geometry the angel θ_B is between $145^o < \theta_B < 180^o$. The angle θ_T and θ_R are known as the look angle of transmitter and the look angle of receiver respectively. These angles are in positive clockwise rotation from the vector drawn perpendicular to the baseline with its head pointing towards the target. This vector is also taken in north up direction in north-refrenced coordinate system [7]. In bistatic geometry,the bistatic velocity wil be the equivalent of radial velocity, which is the component of target velocity along the bistatic angle bisector [8, 9].

1.7 Literature Review

As discussed in passive radar, the transmitted signals are not designed for radar operation purposes and are not in control. Therefore, to study and analyze the feasibility of communication and broadcast waveforms for diverse radar applications is utmost necessary. Hence, over the years different experimental and theoretical studies have been conducted using analog audio signal FM [11–13, 27], Digital Audio Broadcast (DAB) signals [15, 16, 28],

Digital Video Broadcast (DVB) signals [17–19], Cellular telephone signals like second generation (2G) global system for mobile communication (GSM) signal [20–22], 3G UMTS signal [23–25] and 4G long term evolution (LTE) signals [31–33], wireless fidelity (wifi) signal [6, 34, 35], worldwide interoperability for microwave access (WIMAX) signal [36, 37] and recently wireless regional area network (WRAN) cognitive radio (IEEE 802.22) signal [26].

1.7.1 UMTS Signal and Related work

Universal Mobile Telecommunication System(UMTS) is a 3rd generation cellular network (3G) standard in Europe that has been developed and maintained by 3rd Generation Partnership Project(3GPPP). UMTS [38, 39] has two operational modes i.e Frequency Division Duplexing(FDD) and Time Division Duplexing(TDD). In FDD mode, separate frequency bands are used for uplink and downlink transmission. In TDD mode, same frequency band is time shared between uplink and downlink transmission. FDD mode uses paired spectrum bands in the range of 1885-2025 MHz for uplink stream and 2110-2200 MHZ for downlink stream. Whereas TDD mode uses unpaired spectrum bands in the range of 1900-1920 MHZ for uplink transmission and 2010-2025 MHz for downlink transmission. The bandwidth of UMTS signal is 5MHZ. UMTS uses Wide-band Code Division Multiple Access(W-CDMA) as its air interface with 3.84Mchips/sec chip rate. The Quadrature Phase Shift Keying(QPSK) is used as modulation scheme. The root raised cosine(RRC) filter with roll-off factor of 0.22 is used for pulse shaping. The purpose of UMTS is the provision of high data rate with high spectrum efficiency, sup-

port of asymmetric traffic and packet switched transmission efficiently and effectively [39]. However, UMTS downlink transmitted signal has properties that make it potential illuminator of opportunity. Because of higher bandwidth it has relatively higher range resolution than other signals like GSM, FM and DAB. The usage of orthogonal codes(synchronization, channelization,uplink and downlink scrambling codes) provides a desirable characteristic of low side lobes of ambiguity function(AF). The use of frequency bands from 2110-2170 MHZ makes an easy and effective use of directive antennas. Furthermore, the vast coverage of UMTS on the international territory makes the use of multistatic geometry expedient.

Over the recent years both theoretical and experimental studies have been done for UMTS waveform. In [23, 25], the experimental work has been done to analyze characteristic of UMTS signal using ambiguity function. In [40] comparative study has been conducted in the field to inspect performance of GSM and UMTS signal in presence of clutter. The Cramer-Rao Lower Bound(CRLB) is universally used to find the lower bound on local estimation accuracy of any unbiased estimator. UMTS signals have been further investigated theoretically using AF and CRLB. In [9] the AF and Modified-CRLB(MCRLB) has been derived for target range and velocity by considering both monostatic geometry and bistatic geometry. In this work global resolution is sifted with regard to the mainlobe width and sidelobes. This study is further extended to multistatic configuration in [24] for AF and in [41] for MCRLB. In these work analytical expressions have been derived for AF and MCRLB on target range and velocity in both non-coherent pro-

cessing and coherent processing mode by incorporating another study of [42] on MIMO radar.

1.8 Problem formulation and its significance

In this dissertation, we derive the closed-form expressions of the MCRLBs on the target parameters (position and velocity) when receivers in multi-static configuration exploit the line-of-sight component from the target with underlying UMTS signal. For practical situations, we make use of a three dimensional (3D) Euclidean geometry and provide the estimation error bounds for the 3D Euclidean components of the target's position and velocity. From a theoretical point of view, the geometry plays a significant role in improving the performance of estimation whose information is embedded in the Jacobian of the parameters transformation. On the other hand, the relatively smaller values of the MFIM on the parameters of Doppler and delay can give rise to an ill-conditioned matrix. Therefore it is necessary to theoretically prove the existence of a consistent inverse which we establish by showing the positive-definiteness of the total MFIM over all transceiver pairs. Besides, the main motivation of this study is two-folds, which is given below.

Firstly, although the UMTS signal offers many advantages as an illuminator of opportunity for passive radar, it also has a key drawback of transmitting low power from the base transceiver station (BTS). The problem gets worse in case of a UMTS signal as the effective isotropic radiated power is much lower than other signals like GSM, DAB and DVB [5]. An obvious

reason is that the UMTS is based on CDMA in which the users transmit their data simultaneously, therefore, to avoid the so-called *near-far* effect and to achieve power efficiency, the BTS transmits at lowest possible power level [39]. This results in potentially decreasing the signal-to-noise ratio (SNR) required for accurate detection of the target and the estimation of the required parameters at the radar receiver. The further reduction in SNR occurs due to low target RCS values because of non-LoS link between the target and the receiver.

Since the only parameter that can be controlled in radar design is radar cross section (RCS) [48] which varies with variation in receiver position. Although, the transmit power cannot be increased to achieve required SNR, the desired SNR level can be approached by the selection of a suitable geometry for the radar receiver where the dominant or fixed amplitude (LoS) scatterer component coexist with weak (NLoS) scatterer (reflections, echoes) components. The reception of LoS component increases the SNR due to increase in the target RCS values, which results in better accuracy of target's detection and parameter estimation. Further improvement can come by setting the antenna orientation in such away that whole trajectory of target comes in main lobe, direct signal comes in back lobe for its complete attenuation and clutter filter removes all zero doppler echoes this will reduce the interference noise. These tasks are explained in [43–45]. Thus, a suitable solution to the problem of low transmit power is analyzed and lower bounds of MCRLBs are given on the performance improvement.

Secondly, the modeling of target behavior is cumbersome as almost all

targets including simple scatterer to a complex one have variations in RCS because of the variation in aspect angle, frequency and polarization [46]. Moreover, for different applications, the target RCS has different characteristics. Therefore, it is of prime importance to test the performance of a waveform for a broader range of target RCS models. For instance, it is well known that the vast theory of detection and estimation for radar is developed based on the results obtained by the exploitation of famous Swerling models of target RCS fluctuations [46–48], which include Swerling $0 - V$ models. Swerling 0 & V have fixed amplitude RCS values whereas Swerling I & II have pure Rayleigh RCS fluctuations from scan-to-scan and pulse-to-pulse, respectively. Swerling III & IV have fluctuations of one large fixed amplitude scatterer and many small scatterers from scan-to-scan and pulse-to-pulse. Airplanes and ships are practical examples of Swerling I/II and Swerling III/IV, respectively. Similarly, Swerling I & III are known for tracking radars and Swerling II & IV are famous to search radar applications. Therefore, to cover this broader range of target RCS models, either Nakagami or Rician distribution is used. In this work, we use the Rician target model because it provides more insightful depiction of target models [49]. Thus, along with addressing the problem of low transmit power, this study also provides a framework to evaluate the performance limits of a waveform for a broader range of target models, which are known as generalized RCS models (GRCSMs) [49].

1.9 Contributions

Based on analysis of problems and its solutions in the above section, we summarized our contributions as follows:

- Derivation of PDF for target in a LoS environment.
- Derivation of closed-form expressions of MCRLBS on Euclidean components of position and velocity of the target.
- Proof is given that MCRLB matrix is positive-definite.
- Two theorems have been developed to directly determine the MCRLBs on position and velocity of the target lying in LoS environment.
- Analytical framework to evaluate a waveform performance for different target models appears in different radar applications.
- Soltuion to a basic problem of ill-conditioning of inverse matrix in radar applications.

1.10 Thesis Organization

The remaining dissertation is structured as follows. Signal model is presented in Chapter II. MCRLBs expressions for target position and velocity are computed in Chapter III and their numerical evaluations are given in Chapter IV, respectively. Finally, Chapter V concludes the dissertation.

Chapter 2

Signal Model

Consider a multistatic passive radar configuration in a 3D Euclidean space consisting of M_T transmitters, M_R receivers and a single target. Suppose the transmitters and the receivers are located at positions $\mathbf{T}_i = (t_{x_i}, t_{y_i}, t_{z_i})$ and $\mathbf{R}_j = (r_{x_j}, r_{y_j}, r_{z_j})$, where $i = [1, 2, ..., M_T]$ and $j = [1, 2, ..., M_R]$, respectively. Let the target's position is denoted as $\mathbb{T}_p = (p_x, p_y, p_z)$, whereas its velocity is given by $\mathbb{T}_v = (v_x, v_y, v_z)$, where we use the symbol $\mathbb{T}$ to represent the target and the subscripts p and v distinguish its position and velocity, respectively. The vector of parameters of interest is $\mathbf{\Theta} = [p_x, p_y, p_z, v_x, v_y, v_z]$. The signal transmitted by the i^{th} transmitter is given as

$$u_i(t) = \frac{1}{\sqrt{N}} \sum_{n=0}^{N-1} c_{in} g_i \left(t - nT\right), \tag{2.1}$$

where c_{in} denotes the n^{th} transmitted QPSK symbol, N is the total number of symbols in a waveform, and T is the symbol time. For independent and

non-identically distributed symbols we have

$$\mathbb{E}(c_{in}c_{ik}^{*}) = \begin{cases} 1, & n = k \\ \mathbb{E}(c_{in})\mathbb{E}(c_{ik}^{*}), & n \neq k, \end{cases} \tag{2.2}$$

whereas for independent and identical distributed (IID) symbols we will have $\mathbb{E}(c_{in}) = \mathbb{E}(c_{ik}^{*}) = 0$. These symbols are modulated with delayed root-raised cosine (RRC) pulses given as

$$g_i(t) = h_i\left(t - \frac{D}{2}\right), \tag{2.3}$$

where $h_i(t)$ is defined as

$$h(t) = \begin{cases} \frac{1}{\sqrt{T}}(1 - \alpha + \frac{4\alpha}{\pi}), \ t = 0 \\ \frac{\alpha}{\sqrt{2T}}\left[\left(1 + \frac{2}{\pi}\right)\sin\left(\frac{\pi}{4\alpha}\right) + \left(1 - \frac{2}{\pi}\right)\cos\left(\frac{\pi}{4\alpha}\right)\right], \ t = \pm\frac{T}{4\alpha} \\ \frac{\sin((\pi t/T)(1-\alpha)) + (4\alpha t/T)\cos((\pi t/T)(1+\alpha))}{\left(\pi t/\sqrt{T}\right)\left[1-((4\alpha t/T))^2\right]}, \ \text{otherwise.} \end{cases} \tag{2.4}$$

where $h_i(t)$ is plotted in Fig. 2.1 for different values of α

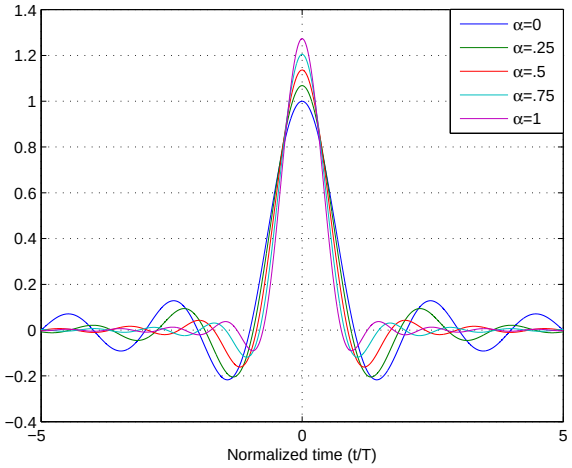

Figure 2.1: Impulse response of an RRC pulse for different values of α.

In (2.4) α is the roll-off (excess bandwidth) factor where $0 \leq \alpha \leq 1$. In (2.3), the delay D is defined such that

$$\int_{-D/2}^{D/2} h^2(t)dt \approx 1. \tag{2.5}$$

The fourier transform of the RRC pulse h(t) is given by H(f) such that

$$H(f) = \sqrt{C(f)} \tag{2.6}$$

where C(f) is

$$C(f) = \begin{cases} T, \ |f| \leq \frac{1-\alpha}{2T} \\ \frac{T}{2}\left[1 + cos\left(\frac{\pi T}{\alpha}\left(|f| - \frac{1-\alpha}{2T}\right)\right)\right], \ \frac{1-\alpha}{2T} \leq \frac{1+\alpha}{2T} \\ 0, \ elswhere \end{cases} \tag{2.7}$$

the inverse fourier transform(IFT) of C(f) is

$$c(t) = IFT(C(f)) = sinc\left(\frac{t}{T}\right)\frac{\cos(\alpha\pi t)}{T}1 - \left(2\alpha t/T\right)^2 \tag{2.8}$$

Since, the RRC pulse is an orthogonal pulse under T-shifts [50], therefore,

$$\begin{cases} \int_{-\infty}^{\infty} g_i\left(t-nT\right) g_i\left(t-kT\right) = 0, & n \neq k \\ \int_{-\infty}^{\infty} g_i\left(t-nT\right) g_i\left(t-kT\right) = \int_{-\infty}^{\infty} h^2(t)dt, & n = k. \end{cases} \tag{2.9}$$

By using the Parseval's theorem, it can easily be verified that

$$\int_{-\infty}^{\infty} h^2(t)dt = \int_{-\infty}^{\infty} H^2(f)df = \int_{-\infty}^{\infty} C(f)df = 1. \tag{2.10}$$

Assume that due to widely spaced antennas, each transmitter-receiver pair has its own aspect angle (angle of view) for the target and thus each of them has its own attenuation factor. Furthermore, assume that signals from different transmitters can be separated at each receiver in some orthogonal domain, for example, in frequency domain due to different spectrums as per [41]. Then by using the Rician target model, the signal from the i^{th} transmitter arriving at the j^{th} receiver in the presence of noise is given as

$$y_{ij}(t) = \beta_{ij}u_i(t-\tau_{ij})e^{-j2\pi f_{D_{ij}}(t-\tau_{ij})} + w_{ij}(t), \tag{2.11}$$

where β_{ij} is the attenuation (reflection) coefficient. For Rician target, this is composed of a fixed amplitude scatterer and many independent isotropic scatterers and is modeled as a complex Gaussian random variable with mean

m_{ij} and variance σ^2, i.e., $\beta_{ij} \sim CN(m_{ij}, \sigma^2)$. The $w_{ij}(t)$ is the additive white Gaussian noise (AWGN) with zero mean and variance σ_n^2 i.e., $w_{ij} \sim CN(0, \sigma_n^2)$. The reflection coefficient β_{ij} and noise $w_{ij}(t)$ are independent of each other. The parameters m_{ij}, σ^2 and σ_n^2 are assumed to be deterministic and known. The delay τ_{ij} and doppler shift $f_{D_{ij}}$ associated with $i-j^{th}$ path are defined as

$$\tau_{ij} = \frac{|\mathbf{T}_i\mathbb{T}_p|+|\mathbf{R}_j\mathbb{T}_p|}{c}\,, \tag{2.12}$$

$$f_{D_{ij}} = \frac{(\mathbb{T}_p\mathbf{R}_j)\cdot\mathbb{T}_v}{\lambda|\mathbf{R}_j\mathbb{T}_p|} + \frac{(\mathbb{T}_p\mathbf{T}_i)\cdot\mathbb{T}_v}{\lambda|\mathbf{T}_i\mathbb{T}_p|}\,, \tag{2.13}$$

where λ is the carrier wavelength, c is the speed of light, $|\mathbf{T}_i\mathbb{T}_p|$ is the Euclidean distance from the i^{th} transmitter to the target and $|\mathbf{R}_j\mathbb{T}_p|$ is the Euclidean distance from the target to the j^{th} receiver, respectively. The $|\mathbf{T}_i\mathbb{T}_p|$ and $|\mathbf{R}_j\mathbb{T}_p|$ are given as

$$|\mathbf{T}_i\mathbb{T}_p| = \sqrt{(p_x - t_{x_i})^2 + (p_y - t_{y_i})^2 + (p_z - t_{z_i})^2}\,, \tag{2.14}$$

$$|\mathbf{R}_j\mathbb{T}_p| = \sqrt{(p_x - r_{x_j})^2 + (p_y - r_{y_j})^2 + (p_z - r_{z_j})^2}\,. \tag{2.15}$$

Following the concepts in [51], the likelihood of a single transmitter-receiver

pair is derived, the logarithm of which is given by

$$\begin{aligned}
&\log \wedge(y_{ij}(t)|\mathbf{c}) = \\
&\frac{\sigma^2}{\sigma_n^2+\sigma^2}\left|\int_{-\infty}^{\infty} y_{ij}(t)\overset{*}{u}_i(t-\tau_{ij})e^{-j2\pi f_{D_{ij}}(t-\tau_{ij})}dt\right|^2 - \\
&\frac{1}{\sigma^2+\sigma_n^2}\left|\int_{-\infty}^{\infty} m_{y_{ij}}\overset{*}{u}_i(t-\tau_{ij})e^{-j2\pi f_{D_{ij}}(t-\tau_{ij})}dt\right|^2 + \\
&\frac{2}{(\sigma^2+\sigma_n^2)}\Re\left(\int_{-\infty}^{\infty} y_{ij}(t)\overset{*}{u}_i(t-\tau_{ij})e^{-j2\pi f_{D_{ij}}(t-\tau_{ij})}dt\times\right. \\
&\left.\int_{-\infty}^{\infty} m^*_{y_{ij}}u_i(t-\tau_{ij})e^{j2\pi f_{D_{ij}}(t-\tau_{ij})}dt\right) + \ln C, \qquad (2.16)
\end{aligned}$$

where $m_{y_{ij}} = m_{ij}u_i(t-\tau_{ij})e^{j2\pi f_{D_{ij}}(t-\tau_{ij})}$ is the mean of the received signal $y_{ij}(t)$, $\Re(.)$ is the real part, $|.|$ is the absolute operator and $(.)^*$ is the conjugation operator. The joint likelihood over M_TM_R transceiver pair is the product of all single transceiver pair likelihoods, i.e.,

$$\Lambda\left(\mathbf{y}(t)|\mathbf{c}\right) = \prod_{i=1}^{M_T}\prod_{j=1}^{M_R} \wedge\left(y_{ij}(t)|\mathbf{c}\right). \qquad (2.17)$$

Therefore, the joint log likelihood is the sum of individual log likelihoods and is given by

$$\log\Lambda\left(\mathbf{y}(t)|\mathbf{c}\right) = \sum_{i=1}^{M_T}\sum_{j=1}^{M_R} \log\wedge\left(y_{ij}(t)|\mathbf{c}\right). \qquad (2.18)$$

Chapter 3

Derivation of MCRLB

The Cramer-Rao Lower Bound (CRLB) is universally used to find the lower bound on the local estimation accuracy of any unbiased estimator. In the classical CRLB, the expectation is taken on the joint probability distribution function (PDF) of the received signal and the parameter vector. Whereas, in modified CRLB (MCRLB) the conditional PDF of the received signal conditioned on transmitted symbols is used. Because of the randomness of the transmitted symbols the classical CRLB is not feasible in our study [9]. The situations in which classical CRLB is not feasible, the MCLRB is considered as a good alternative and is easier to calculate [9, 52]. The relationship between CRLB and MCRLB is discussed in [52–54] and it is shown that MCRLB is a looser bound than the CRLB. Since, it is easier to work with the derivatives of τ and f_D, therefore, we first find the modified Fisher information matrix (MFIM) for parameter vector $\Phi = [\tau_{ij}, f_{D_{ij}}] \; \forall \; i, j$.

To do so, we first write the expression in (2.16) in a simplified form as

$$\log \Lambda(\mathbf{y}; \mathbf{\Phi}|\mathbf{c}) = \sum_{i=1}^{M_T} \sum_{j=1}^{M_R} (\Gamma_{ij} - \Pi_{ij} + \Sigma_{ij}) + \ln C, \tag{3.1}$$

where Γ_{ij}, Π_{ij} and Σ_{ij} are the first, second and third terms in (2.16), respectively. For a single transceiver pair, the MFIM $\mathbf{F}_{ij}^{\mathbf{y}}(\mathbf{\Phi})$, is calculated using the expectation

$$\mathbf{F}_{ij}^{\mathbf{y}}(\mathbf{\Phi}) = -\mathbb{E}_{[\mathbf{y};\, \mathbf{\Phi}|\mathbf{c}]} \Bigg(\nabla_{\mathbf{\Phi}} [\nabla_{\mathbf{\Phi}} \log \Lambda(\mathbf{y}; \mathbf{\Phi}|\mathbf{c})] \Bigg), \tag{3.2}$$

where $\nabla_{\mathbf{\Phi}}$, is the first-order linear derivative and $\mathbb{E}[.]$ denotes the expectation operator. Due to linearity of second-order derivatives, it immediately follows that total MFIM is the sum of individual MFIMs which is shown in the following proposition.

Proposition 1. *Let* $\boldsymbol{F}_{ij}^{\mathbf{\Gamma}}$, $\boldsymbol{F}_{ij}^{\mathbf{\Pi}}$, *and* $\boldsymbol{F}_{ij}^{\mathbf{\Sigma}}$, *denote the MFIMs corresponding to the terms* Γ_{ij}, Π_{ij} *and* Σ_{ij}, *respectively then the total MFIM* $\boldsymbol{F}^{\boldsymbol{y}}(\mathbf{\Phi})$ *over all transceiver pairs in a LoS environment is a linear combination of the components contributing from both LoS and NLoS and is given by*

$$\mathbf{F}^{\mathbf{y}}(\mathbf{\Phi}) = \sum_{i=1}^{M_T} \sum_{j=1}^{M_R} \mathbf{F}^{\mathbf{y}}(\mathbf{\Phi})_{ij} = \sum_{i=1}^{M_T} \sum_{j=1}^{M_R} \left(\mathbf{F}_{ij}^{\mathbf{\Gamma}}(\mathbf{\Phi}) + \mathbf{F}_{ij}^{\mathbf{\Pi}}(\mathbf{\Phi}) + \mathbf{F}_{ij}^{\mathbf{\Sigma}}(\mathbf{\Phi}) \right). \tag{3.3}$$

Proof. Due to linearity, the derivatives of each term in Eq. (3.1) can be calculated separately. Thus, the required MFIM $\mathbf{F}^{\mathbf{y}}(\mathbf{\Phi})$, can be expressed as

a linear combination of the three terms as

$$\begin{aligned}
\mathbf{F}^{\mathbf{y}}(\mathbf{\Phi}) &= -\,\mathbb{E}_{[\mathbf{y};\,\mathbf{\Phi}|\mathbf{c}]}\Big(\nabla_{\mathbf{\Phi}}[\nabla_{\mathbf{\Phi}}\log\Lambda(\mathbf{y};\mathbf{\Phi}|\mathbf{c})]\Big),\\
&= -\,\mathbb{E}_{[\mathbf{y};\,\mathbf{\Phi}|\mathbf{c}]}\left(\nabla_{\mathbf{\Phi}}\nabla_{\mathbf{\Phi}}\Big(\sum_{i=1}^{M_T}\sum_{j=1}^{M_R}(\Gamma_{ij}-\Pi_{ij}+\Sigma_{ij})\Big)\right),\\
&= -\,\mathbb{E}_{[\mathbf{y};\,\mathbf{\Phi}|\mathbf{c}]}\left(\sum_{i=1}^{M_T}\sum_{j=1}^{M_R}\left(\nabla_{\mathbf{\Phi}}\nabla_{\mathbf{\Phi}}\Gamma_{ij}-\nabla_{\mathbf{\Phi}}\nabla_{\mathbf{\Phi}}\Pi_{ij}\right.\right.\\
&\qquad\left.\left.+\,\nabla_{\mathbf{\Phi}}\nabla_{\mathbf{\Phi}}\Sigma_{ij}\right)\right),
\end{aligned}\tag{3.4}$$

which are the corresponding MFIMs over all the terms Γ_{ij}, Π_{ij} and Σ_{ij}, respectively, which completes the proof of Proposition 1. We now calculate the MFIM corresponding to the terms Γ_{ij}, Σ_{ij} and Π_{ij}, from the original likelihood function by evaluating all the second-order derivatives followed up by their expectations. It turns out that the MFIM contribution from the term Γ_{ij} is the sum of the contribution of two terms, i.e., $\Gamma_{ij}^{(NLoS)}$ and $\Gamma_{ij}^{(LoS)}$, where the term $\Gamma_{ij}^{(NLoS)}$ contribute to MFIM due to NLoS component and $\Gamma_{ij}^{(LoS)}$ contribute to MFIM due to LoS component, respectively. The terms Σ_{ij} and Π_{ij} only contribute to MFIM due to LoS components. The MFIMs due to the terms $\Gamma_{ij}^{(LoS)}$, Σ_{ij}, and Π_{ij} are the scalar multiples of the MFIM due to $\Gamma_{ij}^{(NLoS)}$ which is shown in the following theorem.

Theorem 1. *The total MFIM* $\mathbf{F}^{\mathbf{y}}(\mathbf{\Phi})_{ij}$ *obtained by the received signal over a single transceiver pair in the presence of LoS is a linear combination of the four terms, i.e.,* $\mathbf{F}^{\mathbf{\Gamma}\,(\mathbf{NLoS})}(\mathbf{\Phi})_{ij}$ *which is MFIM due to NLoS component*

and the terms $\mathbf{F}^{\mathbf{\Gamma}}(\mathbf{\Phi})_{ij}$, $\mathbf{F}^{\mathbf{\Sigma}}(\mathbf{\Phi})_{ij}$, *and* $\mathbf{F}^{\mathbf{\Pi}}(\mathbf{\Phi})_{ij}$ *which are MFIMs due to LoS component, such that MFIMs due to later three terms are the scalar multiples of the first term given as*

$$\mathbf{F}_{ij}^{\Gamma\,(NLoS)}(\mathbf{\Phi}) = \frac{8\pi^2(\Upsilon_{NLoS})^2}{1+\Upsilon_{NLoS}} \times \begin{bmatrix} \frac{1}{12\pi^2T^2}\Big(\pi^2+3\alpha^2(\pi^2-8)\Big) & 0 \\ 0 & \frac{T^2}{48\alpha}\Big(3+4\alpha(N^2-1)\Big) \end{bmatrix}, \tag{3.5}$$

$$\mathbf{F}_{ij}^{\Gamma\,(LoS)}(\mathbf{\Phi}) = 2\kappa_{ij}\mathbf{F}_{ij}^{\Gamma\,(NLoS)}(\mathbf{\Phi}), \tag{3.6}$$

$$\mathbf{F}_{ij}^{\Pi}(\mathbf{\Phi}) = \frac{-2\kappa_{ij}}{\Upsilon_{NLoS}}\mathbf{F}_{ij}^{\Gamma\,(NLoS)}(\mathbf{\Phi}), \tag{3.7}$$

$$\mathbf{F}_{ij}^{\Sigma}(\mathbf{\Phi}) = \frac{4\kappa_{ij}}{\Upsilon_{NLoS}}\mathbf{F}_{ij}^{\Gamma\,(NLoS)}(\mathbf{\Phi}). \tag{3.8}$$

Proof. The proof is given in Appendix 1.

Therefore, it is clear from Theorem 1 that the first term is contribution due to NLoS components and other three terms are the contributions from the LoS component. The entries of MFIM $\mathbf{F}_{ij}^{\mathbf{y}}(\mathbf{\Phi})$, are derived in the Appendix 1. Now the MFIM $\mathbf{J}_{ij}(\mathbf{\Theta})$, on the desired parameters of interest, i.e., target's position and velocity $\mathbf{\Theta} = [p_x, p_y, p_z, v_x, v_y, v_z]$, can be obtained easily with an application of chain rule. It is easy to see that the chain rule implies the existence of the Jacobian from the space $\mathbf{\Phi} \in \mathbb{R}^2$, to a six-dimensional space $\mathbf{\Theta} \in \mathbb{R}^6$, or equivalently

$$\mathbf{F}_{ij}(\mathbf{\Theta}) = \left(\frac{\partial \mathbf{\Phi}}{\partial \mathbf{\Theta}}\right)\mathbf{F}_{ij}^{\mathbf{y}}(\mathbf{\Phi})\left(\frac{\partial \mathbf{\Phi}}{\partial \mathbf{\Theta}}\right)^T. \tag{3.9}$$

Here $\left(\frac{\partial \mathbf{\Phi}}{\partial \mathbf{\Theta}}\right) \in \mathbb{R}^{6\times 2}$ is the Jacobian matrix and its entries are calculated by

taking the derivatives of the delay term in (2.12) and the Doppler term in (2.13) as follows

$$\frac{\partial \tau_{ij}}{\partial p_x} = \frac{1}{c}\left(\frac{p_x - t_{x_i}}{|\mathbf{T}_i \mathbb{T}_p|} + \frac{p_x - r_{x_j}}{|\mathbf{R}_j \mathbb{T}_p|} \right), \tag{3.10}$$

$$\frac{\partial \tau_{ij}}{\partial p_y} = \frac{1}{c}\left(\frac{p_y - t_{y_i}}{|\mathbf{T}_i \mathbb{T}_p|} + \frac{p_y - r_{y_j}}{|\mathbf{R}_j \mathbb{T}_p|} \right), \tag{3.11}$$

$$\frac{\partial \tau_{ij}}{\partial p_z} = \frac{1}{c}\left(\frac{p_z - t_{z_i}}{|\mathbf{T}_i \mathbb{T}_p|} + \frac{p_z - r_{z_j}}{|\mathbf{R}_j \mathbb{T}_p|} \right). \tag{3.12}$$

$$\begin{aligned} \lambda \frac{\partial f_{D_{ij}}}{\partial p_x} = & -\frac{v_x}{|\mathbf{R}_j \mathbb{T}_p|} - \frac{v_x}{|\mathbf{T}_i \mathbb{T}_p|} - \\ & - \frac{(p_x - r_{x_j})((r_{x_j} - p_x)v_x + (r_{y_j} - p_y)v_y + (r_{z_j} - p_z)v_z)}{|\mathbf{R}_j \mathbb{T}_p|^3} \\ & - \frac{(p_x - t_{x_i})((t_{x_i} - p_x)v_x + (t_{y_i} - p_y)v_y + (t_{z_i} - p_z)v_z)}{|\mathbf{T}_i \mathbb{T}_p|^3}, \end{aligned} \tag{3.13}$$

$$\begin{aligned} \lambda \frac{\partial f_{D_{ij}}}{\partial p_y} = & -\frac{v_y}{|\mathbf{R}_j \mathbb{T}_p|} - \frac{v_y}{|\mathbf{T}_i \mathbb{T}_p|} - \\ & - \frac{(p_y - r_{y_j})((r_{x_j} - p_x)v_x + (r_{y_j} - p_y)v_y + (r_{z_j} - p_z)v_z)}{|\mathbf{R}_j \mathbb{T}_p|^3} \\ & - \frac{(p_y - t_{y_i})((t_{x_i} - p_x)v_x + (t_{y_i} - p_y)v_y + (t_{z_i} - p_z)v_z)}{|\mathbf{T}_i \mathbb{T}_p|^3}, \end{aligned} \tag{3.14}$$

$$\lambda\frac{\partial f_{D_{ij}}}{\partial p_z} = -\frac{v_z}{|\mathbf{R}_j\mathbb{T}_p|} - \frac{v_z}{|\mathbf{T}_i\mathbb{T}_p|} - \\ -\frac{(p_z - r_{z_j})((r_{x_j} - p_x)v_x + (r_{y_j} - p_y)v_y + (r_{z_j} - p_z)v_z)}{|\mathbf{R}_j\mathbb{T}_p|^3} \\ -\frac{(p_z - t_{z_i})((t_{x_i} - p_x)v_x + (t_{y_i} - p_y)v_y + (t_{z_i} - p_z)v_z)}{|\mathbf{T}_i\mathbb{T}_p|^3}\,. \tag{3.15}$$

Similarly the first-order derivatives with respect to velocities are

$$\lambda\frac{\partial f_{D_{ij}}}{\partial v_x} = \frac{t_{x_i} - p_x}{|\mathbf{T}_i\mathbb{T}_p|} + \frac{r_{x_j} - p_x}{|\mathbf{R}_j\mathbb{T}_p|}\,, \tag{3.16}$$

$$\lambda\frac{\partial f_{D_{ij}}}{\partial v_y} = \frac{t_{y_i} - p_y}{|\mathbf{T}_i\mathbb{T}_p|} + \frac{r_{y_j} - p_y}{|\mathbf{R}_j\mathbb{T}_p|}\,, \tag{3.17}$$

$$\lambda\frac{\partial f_{D_{ij}}}{\partial v_z} = \frac{t_{z_i} - p_z}{|\mathbf{T}_i\mathbb{T}_p|} + \frac{r_{z_j} - p_z}{|\mathbf{R}_j\mathbb{T}_p|}\,. \tag{3.18}$$

The closed-form expression of the MFIM in (3.9) is given in Appendix 2. Thus, the final expression for total MFIM over all transceiver pairs after all the calculations becomes

$$\mathbf{F}(\mathbf{\Theta}) = \frac{8\pi^2(\Upsilon_{NLoS})}{1 + \Upsilon_{NLoS}} \\ \sum_{i=1}^{M_T}\sum_{j=1}^{M_R}\mathbf{F}_{ij}(\mathbf{\Theta})(\Upsilon_{NLoS} + 2(\Upsilon_{NLoS})\kappa_{ij} + 2\kappa_{ij}). \tag{3.19}$$

where the parameter $\kappa_{ij} = |m_{ij}|^2/2\sigma^2$, expresses the ratio of the power in LoS scatterer to the power in NLoS scatterers. For Rician target or in the presence of LoS environment, the total target SNR ($\Upsilon_{T_{ij}}$) for a single transceiver pair at the receiver will be the sum of the SNR from weak reflections or the NLoS components (Υ_{NLoS}) and SNR from the dominant reflection or LoS

component ($\Upsilon_{LoS_{ij}}$), i.e.,

$$\Upsilon_{T_{ij}} = \Upsilon_{NLoS} + \Upsilon_{LoS_{ij}}. \tag{3.20}$$

where $\Upsilon_{NLoS} = \sigma^2/\sigma_n^2$ and $\Upsilon_{LoS_{ij}} = |m_{ij}|^2/2\sigma_n^2$. We also develop a relationship between κ_{ij} to another parameter, introduced here as κ'_{ij}, and defined in [49] as $\kappa'_{ij} = \Upsilon_{LoS_{ij}}/\Upsilon_{T_{ij}}$. Thus, after some algebraic manipulation it turns out that

$$\kappa'_{ij} = \frac{\kappa_{ij}}{1+\kappa_{ij}}, \tag{3.21}$$

where $0 \leq \kappa'_{ij} \leq 1$, is used for the categorization of the target RCS models. For instance, the Swerling-I/II models, Swerling-III/IV models and Swerling-$0/V$ model corresponds to the value of $\kappa'_{ij} = 0, 0.75$ and 1, respectively. This leads to the evaluation of the feasibility of a waveform for a broader range of radar applications in a unified framework. Also as in [41] where MCRLB is calculated for non-coherent and coherent modes separately, the specialized cases corresponding to $\kappa'_{ij} = 0$ and 1, respectively attribute to the same phenomena. From Eq. (3.19), it is obvious that MFIM depends on a number of factors. On one hand, it is strongly dependant on the geometry, which incorporates the positions of the transmitters, receivers and target in a Euclidean space. On the other hand, it also depends on the properties of the waveform such as RRC roll-off factor, number of symbols and symbol time. Moreover, it also shows strong dependence on the target RCS and SNR.

Computational Remarks. It is important to mention that while obtaining the MCRLB on the parameters of interest, it is desired to take the

inverse of MFIM which at times becomes a hard task if the resulting MFIM is an ill-conditioned matrix. The situation of an ill-conditioned matrix arises mainly because the first-order derivatives of both Doppler and delay primarily contains the term $1/\lambda$ and $1/c$, which are of the orders of $\sim 10^{-10}$ and $\sim 10^{-8}$, respectively. Since the required MFIM (see Appendix 2) depends quadratically on the first-order derivatives, therefore, the matrix $\mathbf{F}_{ij}(\boldsymbol{\Theta})$, contains some off-diagonal entries of the order of $\sim 10^{-20}$, resulting severe floating point and truncation errors in advanced computer algebra systems (MATLAB OR MATHEMATICA). In the favorable circumstances, if a matrix is well-behaved then the condition number is of order one. It turns out that the condition number of the matrix $\mathbf{F}_{ij}(\boldsymbol{\Theta})$, in such cases is of the order 10^{22}, which is quite large. In the aforementioned situation, we have to use one of the many available algorithms to find the inverse of an ill-conditioned matrix in a consistent manner in a computer algebra system. To obtain the required MCRLB over target parameters it is necessary to prove the existence of a consistent inverse of total MFIM $\mathbf{F}(\boldsymbol{\Theta})$, summed over all transceiver pairs.

Since the matrix $\mathbf{F}(\boldsymbol{\Theta})$, is a 6×6 symmetric matrix and plays a significant role in calculating the desired MCRLB, therefore, it is important to investigate its characteristics in terms of eigen values, Cholesky decomposition and positive-definiteness. The following theorem confirms the positive-definiteness of the total MFIM over all transceiver pairs which we prove using standard results from linear algebra [55].

Theorem 2. *The total MFIM $\boldsymbol{F}(\boldsymbol{\Theta})$ for all transceiver pairs is a positive-*

$$\mathbf{\Omega}^3 = \frac{8\pi^2(\Upsilon_{NLoS})}{1+\Upsilon_{NLoS}} F^{22} \begin{bmatrix} \sum_{i,j} \tilde{\kappa}_{ij} f^2_{Dij,v_x} & \sum_{i,j} \tilde{\kappa}_{ij} f_{Dij,v_x} f_{Dij,v_y} & \sum_{i,j} \tilde{\kappa}_{ij} f_{ij,v_x} f_{Dij,v_z} \\ \sum_{i,j} \tilde{\kappa}_{ij} f_{Dij,v_x} f_{Dij,v_y} & \sum_{i,j} \tilde{\kappa}_{ij} f^2_{Dij,v_y} & \sum_{i,j} \tilde{\kappa}_{ij} f_{Dij,v_y} f_{Dij,v_z} \\ \sum_{i,j} \tilde{\kappa}_{ij} f_{ij,v_x} f_{Dij,v_z} & \sum_{i,j} \tilde{\kappa}_{ij} f_{Dij,v_y} f_{Dij,v_z} & \sum_{i,j} \tilde{\kappa}_{ij} f^2_{Dij,v_z} \end{bmatrix}, \tag{3.23}$$

definite matrix with all of its eigenvalues real and positive.

Proof. As the matrix $\mathbf{F}(\mathbf{\Theta}\ )$ is symmetric, therefore, all of its eigenvalues are real. We need to show that it does not contain a negative eigenvalue. In order to do that, we prove the Schur complement condition for positive definiteness. We first write the MFIM in a block matrix form

$$\mathbf{F}(\mathbf{\Theta}) = \begin{bmatrix} \mathbf{\Omega}^1 & \mathbf{\Omega}^2 \\ \mathbf{\Omega}^{2^T} & \mathbf{\Omega}^3 \end{bmatrix}, \tag{3.22}$$

where each $\mathbf{\Omega}^i$, $\forall\ i = \{1,2,3\}$, is a 3×3 symmetric matrix. Therefore, by Schur's Lemma, the MFIM is positive-definite ($\mathbf{F}(\mathbf{\Theta}) \succeq 0$) if and only if the matrix $\mathbf{\Omega}^3 \succeq 0$ and the Schur complement $\mathbf{\Omega}^1 - \mathbf{\Omega}^{2^T}\mathbf{\Omega}^{\mathbf{3}^{-1}}\mathbf{\Omega}^2 \succeq 0$, are both positive-definite. We establish the positive definiteness of $\mathbf{\Omega}^3$ in the following lemma.

Lemma 1. *The symmetric matrix $\mathbf{\Omega}^3$ is a positive definite matrix.*

Proof. Using the results in Appendix 2, the explicit form of $\mathbf{\Omega}^3$ is given in Eq. (3.23) at the top of subsequent column where $\tilde{\kappa}_{ij} = \Upsilon_{NLoS} + 2(\Upsilon_{NLoS})\kappa_{ij} + 2\kappa_{ij}$ and the factor F^{22}, is the second diagonal term in Eq. (3.5). We now use the Gershgorin circle theorem, which states that every eigenvalue of a square matrix lies within at least one of the Gershgorin discs $D(\mathbf{\Omega}^3_{ii}, R_i)$, where $\mathbf{\Omega}^3_{ii}$ are the diagonal entries and $R_i = \sum_{j\neq i} |\mathbf{\Omega}^3_{ij}|$, are the radii of discs.

From the above equation, it is clear that $\mathbf{\Omega}^3_{ii} > 0$, for all i. Moreover all leading principal minors of the above matrix have positive determinants, i.e., $\sum_{i,j} \tilde{\kappa}_{ij} f^2_{Dij,v_x} > 0$, and by a simple procedure of mathematical induction the following inequality holds

$$\sum_{i,j} \tilde{\kappa}_{ij} f^2_{Dij,v_x} \sum_{i,j} \tilde{\kappa}_{ij} f^2_{Dij,v_y} > \left(\sum_{i,j} \tilde{\kappa}_{ij} f_{Dij,v_x} f_{Dij,v_y} \right)^2, \tag{3.24}$$

which is true over the sum of all transceiver pairs thus the eigenvalues of above matrix are all positive thereby proving Lemma 1. We now establishes the positive definiteness of the Schur complement in the subsequent lemma.

Lemma 2. *The Schur complement* $\mathbf{\Omega^1} - \mathbf{\Omega^{2}}^T \mathbf{\Omega^{3}}^{-1} \mathbf{\Omega^2}$, *is a positive definite matrix.*

Proof. The proof of the above lemma is given in Appendix 3. This completes the proof of Theorem 2 and provide us theoretical basis for the existence of the inverse of $\mathbf{F}(\mathbf{\Theta})$.

Chapter 4

Numerical Results

For numerical demonstration, we assume five transmitters and an equal number of receivers, i.e., $M_T = 5$ and $M_R = 5$. The Euclidean coordinates of their positions (in Km) are given in Table I. For a brief discussion, we consider two

Table 4.1: Transmitters and Receivers positions (Km)

$\mathbf{T}_i$	$\mathbf{R}_j$
$[2, 2.5, 0.4]$	$[3.5, 0.5, 0.5]$
$[2, 2.75, 0.4]$	$[5, 0.5, 0.5]$
$[2, 3, 1]$	$[0.5, 4, 1.1]$
$[2.5, 2, 1]$	$[1.5, 1.5, 1.1]$
$[2.5, 2.25, 1]$	$[4.5, 4.1, 1.1]$

scenarios in a 3D geometry where the first scenario is visualized in Fig. 4.1. For the simulation parameters, we choose the observation time $NT = 0.1$ sec, $f_c = 2100$ MHz as in [9] and for a UMTS signal $T = 0.26$ μsec and $\alpha = 0.22$. In first scenario, the effects of the variations in LoS contribution on the estimation accuracy is studied by varying κ. Here $\kappa = \kappa_{ij}$, is assumed to be the same for all transceiver pairs without loss of generality. In this

case, the target is assumed to be located at the position $[3.4, 2.5, 3.7]$ Km with velocity $[30, 20, 25]$ m/sec. The square roots of MCRLB (RMCRLBs) are plotted against Υ_{NLoS} for components of target position in Fig. 4.2-4.4, and for components of its velocity in Fig. 4.5-4.7, respectively.

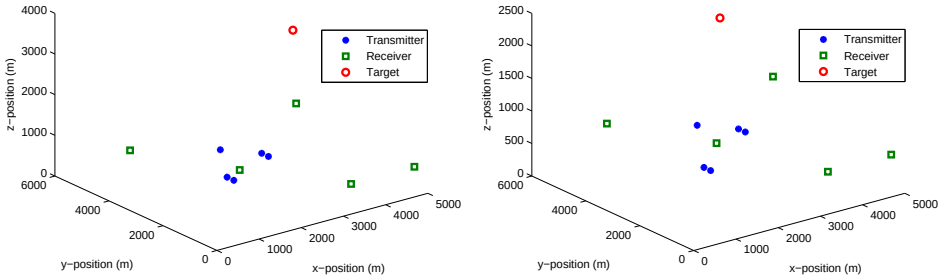

Figure 4.1: Simulated multistatic 3D scenarios 1 and 2 with positions of transmitters $\mathbf{T}_i$, receivers $\mathbf{R}_j$ and target $\mathbb{T}$.

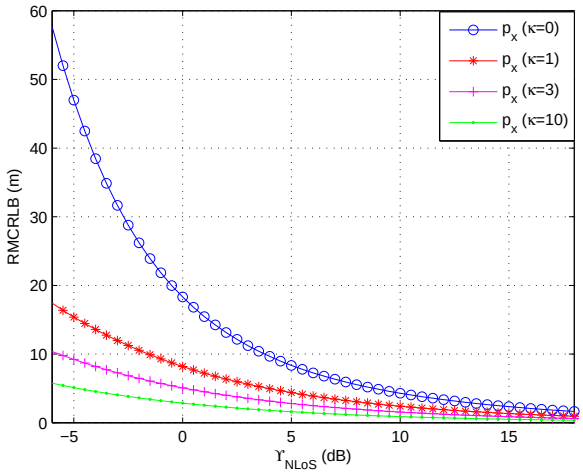

Figure 4.2: RMCRLB variation with κ for x-component of target position $[3.4, 2.5, 3.7]$ (Km).

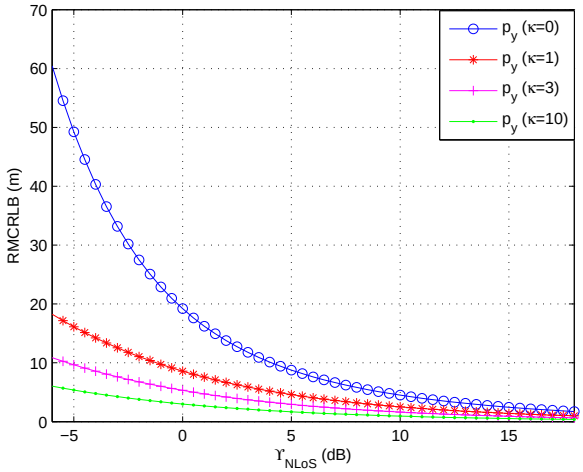

Figure 4.3: RMCRLB variation with κ for y-component of target position $[3.4, 2.5, 3.7]$ (Km).

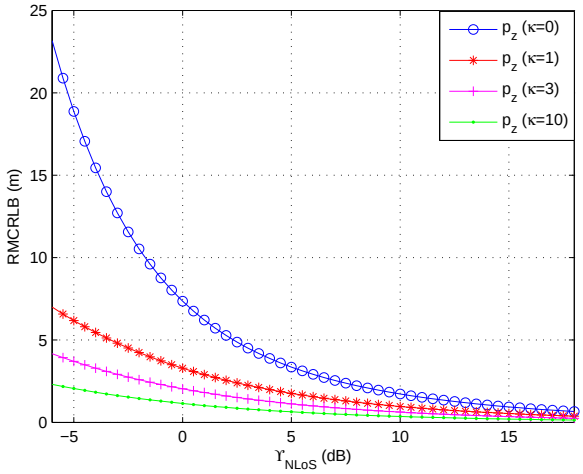

Figure 4.4: RMCRLB variation with κ for z-component of target position $[3.4, 2.5, 3.7]$ (Km).

It is evident from the Figs. 4.2-4.7 that as the value of κ increases, the estimation errors decrease for Euclidean components of target position and velocity. This is because an increase in κ provides a rise in target RCS, which

eventually increases the SNR at the receiver. Consequently, the RMCRLB will achieve a minimum value at an asymptotic limit, i.e., $\kappa \to \infty$, where the target has a fixed amplitude RCS for all transceiver pairs and thus the best estimation accuracy will be achieved. On the contrary, the RMCRLB will be maximum when LoS does not exist at all, i.e., $\kappa \to -\infty$, and target RCS follows a Rayleigh model for all transceiver pairs. For the rest of intermediate cases, the performance lies in between these two limits.

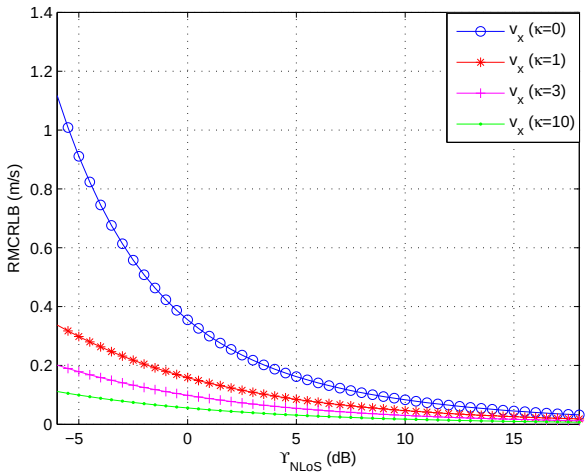

Figure 4.5: RMCRLB variation with κ for x-component of target velocity $[30, 20, 25]$ (m/sec).

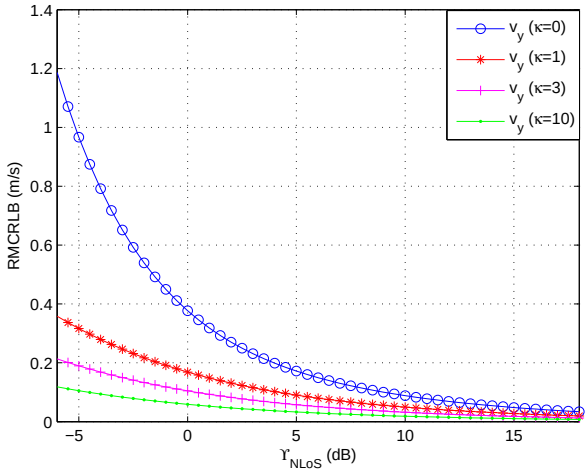

Figure 4.6: RMCRLB variation with κ for y-component of target velocity $[30, 20, 25]$ (m/sec).

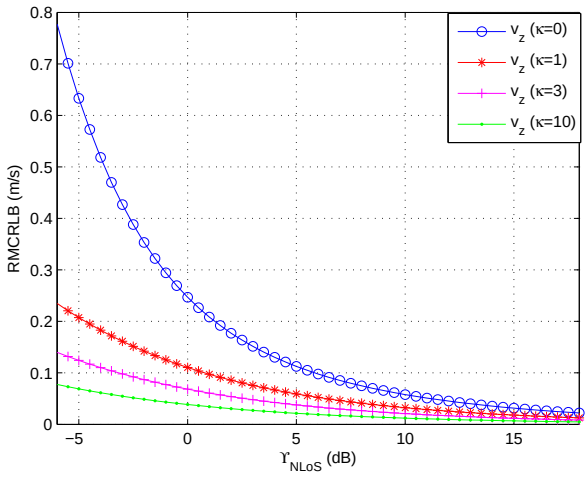

Figure 4.7: RMCRLB variation with κ for z-component of target velocity $[30, 20, 25]$ (m/sec).

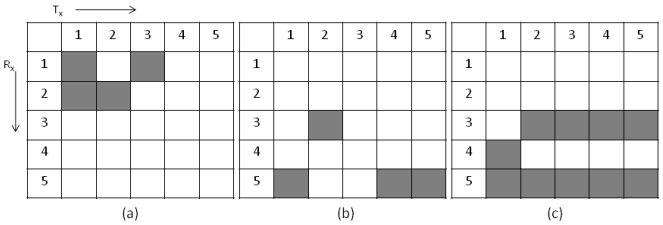

Figure 4.8: Transceiver pairs with and without LoS component.

From a practical point of view, the LoS may exist only for a subset of transceiver pairs. We depict this scenario for various subgroups of transceiver pairs. The existence and absence of LoS among various transceiver pairs is shown in Fig. 4.8, where the filled boxes show the existence of LoS and empty boxes shows its absence. We change the position of the target to $[3.5, 4.5, 2.1]$ Km and its velocity to $[35, 45, 15]$ m/sec to study the effects of geometry as well.

We consider a fixed Swerling-III/IV target model by choosing $\kappa = 3$. In Figs. 4.11 & 4.14, the RMCRLBs are plotted against Υ_{NLoS} for NLoS case and the cases shown in Fig. 4.8. We see that as the number of transceiver pairs with LoS increases, the RMCRLB decreases. For example, the RMCRLB for v_x at -4 dB in Fig. 4.14 is 0.5266 m/sec, 0.4347 m/sec, 0.2284 m/sec, and 0.1536 m/sec for NLoS , Fig. 4.8 (a) case, Fig. 4.8 (b) case and Fig. 4.8 (c) case, respectively. Also we see that the choice of transceiver pair also have significant effect on the estimation accuracy.

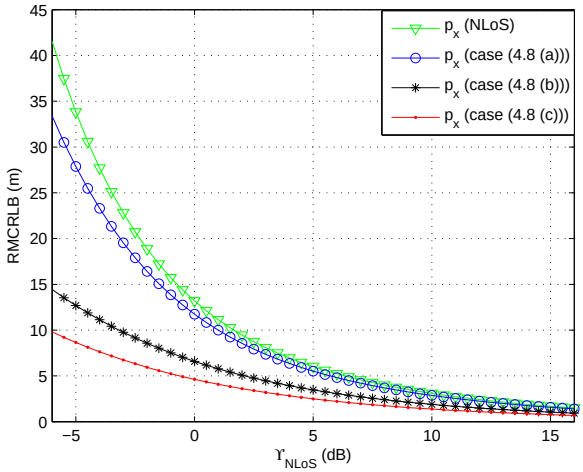

Figure 4.9: RMCRLB vs Υ_{NLoS} for x-component of target position $[3.5, 4.5, 2.1]$ (Km) with various transceiver pairs selection for LoS.

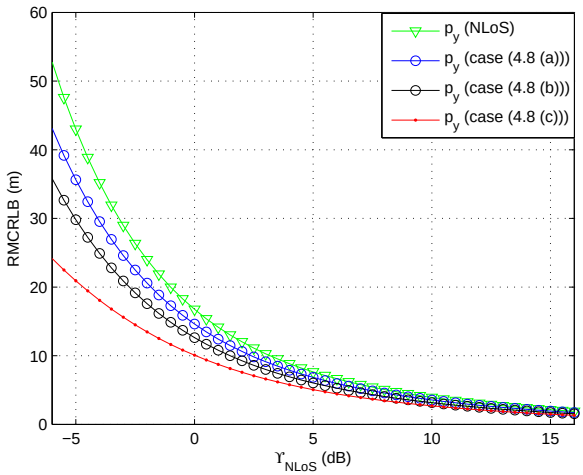

Figure 4.10: RMCRLB vs Υ_{NLoS} for y-component of target position $[3.5, 4.5, 2.1]$ (Km) with various transceiver pairs selection for LoS.

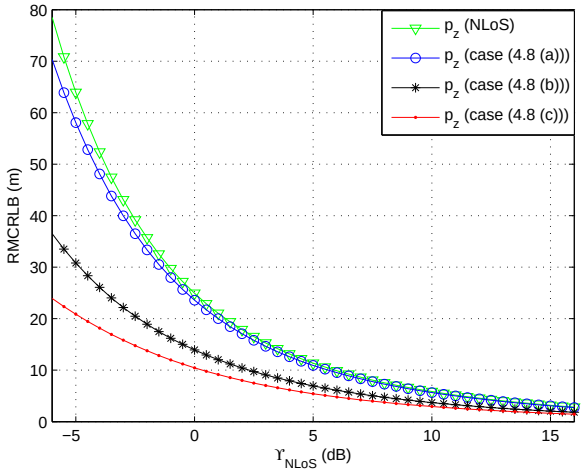

Figure 4.11: RMCRLB vs Υ_{NLoS} for z-component of target position $[3.5, 4.5, 2.1]$ (Km) with various transceiver pairs selection for LoS.

For instance, in Fig. 4.9, for the same number of transceiver pairs, the Fig. 4.8 (c) provides a lower RMCLRB value of 6.586 m than Fig. 4.8 (b) having RMCRLB value of 11.74 m for p_x component. This effect is attributed to the multistatic geometry. Furthermore, in Fig. 4.2 and 4.4, the RMCRLB at -4 dB is 40.32 m for p_x, and 15.45 m for p_z. As the geometry changes by changing the target position and velocity, these values are changed and become 27.7 m for p_x, and 52.35 m for p_z in Fig. 4.9 and 4.11. Also from Fig. 4.2 & 4.4, p_z has lower error values than p_x, however, it has higher error values in Fig. 4.11 than p_x in Fig. 4.9 due to geometry.

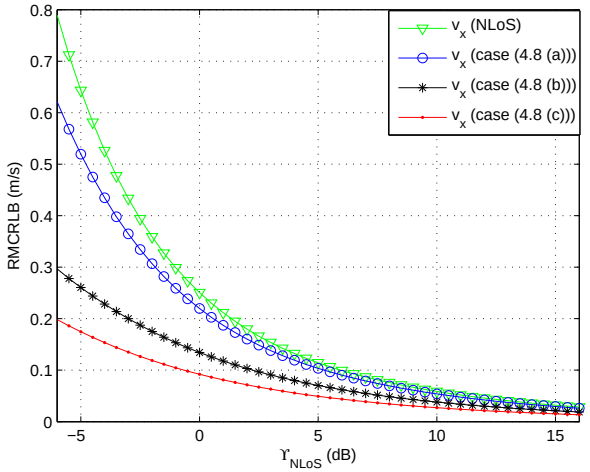

Figure 4.12: RMCRLB vs Υ_{NLoS} for x-component of target velocity $[35, 45, 15]$ (m/sec) with various transceiver pairs selection for LoS.

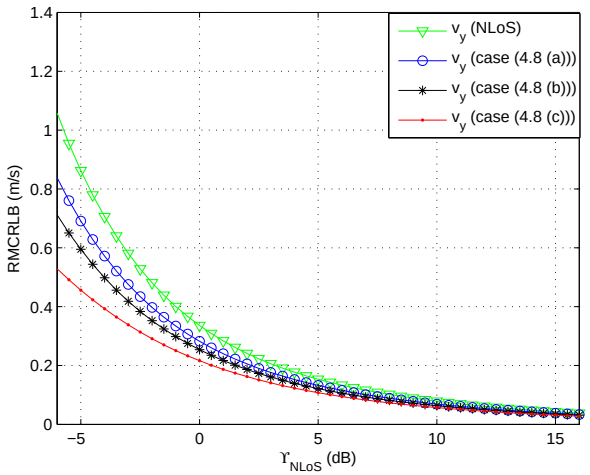

Figure 4.13: RMCRLB vs Υ_{NLoS} for y-component of target velocity $[35, 45, 15]$ (m/sec) with various transceiver pairs selection for LoS.

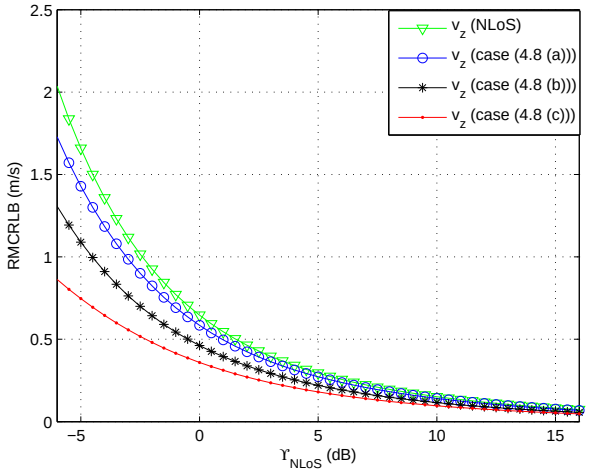

Figure 4.14: RMCRLB vs Υ_{NLoS} for z-component of target velocity $[35, 45, 15]$ (m/sec) with various transceiver pairs selection for LoS.

In Fig. 4.15, the RMCRLBs for position coordinates are plotted against the observation time (NT) at 0 dB for a Rayleigh target ($\kappa = 0$). It can be seen that the RMCRLB decreases with an increase in NT. This indicates that a waveform with a larger data set will provide better performance. However, the obvious disadvantage is that increasing NT will increase the data processing requirement. Moreover, the variation in RMCRLB is not as sensitive as it is to the geometry, SNR and target RCS.

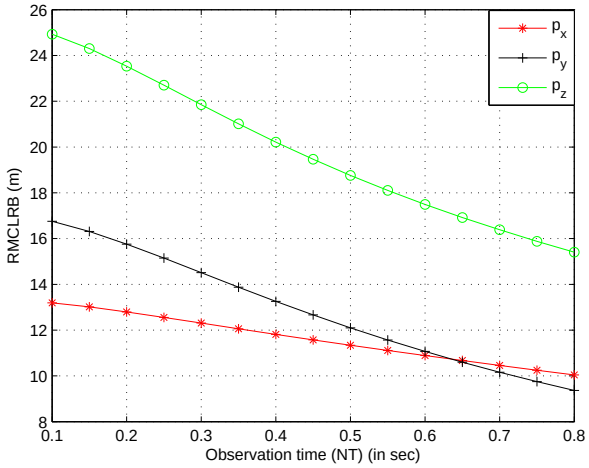

Figure 4.15: RMCRLB vs observation time for target position $[3.5, 4.5, 2.1]$ (Km).

Chapter 5

Concluding Remarks

In this dissertation, we have analyzed the performance of a UMTS-based passive multistatic radar in a LoS environment. The signal model and PDF of the received data have been derived. The closed-form expressions of MCRLBs for the position and velocity have been derived in a 3D Euclidean geometry. It is found that the cumulative MFIM comprises of components due to a fixed amplitude scatterer which is a LoS contribution and weak amplitude scatterers which is the contribution from NLoS component for each transceiver pair. The MFIM depends on waveform properties, SNR, type of target RCS and geometry. With the aid of numerical examples it is shown that estimation accuracy increases with an increase in LoS factor, number of transceiver pairs and/or the choice of the transceiver pairs and observation time. However, it is more sensitive to the LoS factor and/or choice of the transceiver pairs which are strongly linked with the geometry. It shows that by incorporating LoS the waveform can be characterized for GRCSM which includes a broader range of target RCS models appear in different radar applications.

In future, we will use this framework to analyze the performance limits of other illuminators of opportunities like LTE and cognitive radios (IEEE 802.22), etc. Also, we use this work as a case study to develop mathematical relations which can be used to obtain an optimal geometry for increasing the estimation accuracy with arbitrary waveforms and large number of targets.

Appendices

Appendix A

Proof of Theorem 1

Proof of Theorem 1.

From Eq. 2.16, we have

$$\Gamma_{ij} = \frac{\sigma^2}{\sigma_n^2 + \sigma^2} \left| \int_{-\infty}^{\infty} y_{ij}(t) \overset{*}{u}_i(t - \tau_{ij}) e^{-j2\pi f_{D_{ij}}(t-\tau_{ij})} dt \right|^2 .$$

Suppose $\gamma_{ij} = \int_{-\infty}^{\infty} y_{ij}(t) \overset{*}{u}_i(t - \tau_{ij}) e^{-j2\pi f_{D_{ij}}(t-\tau_{ij})} dt$, then from the above expression we determine the first derivative

$$\frac{\partial \Gamma_{ij}}{\partial \tau_{ij}} = \frac{\sigma^2}{\sigma_n^2 + \sigma^2} \left(\frac{\partial \gamma_{ij}}{\partial \tau_{ij}} \gamma_{ij}^* + \gamma_{ij} \frac{\partial \gamma_{ij}^*}{\partial \tau_{ij}} \right). \tag{A.1}$$

The final expression after calculating all the derivatives of γ_{ij} and its conjugate, we obtain

$$\frac{\partial \Gamma_{ij}}{\partial \tau_{ij}} = \frac{2\sigma^2}{\sigma_n^2(\sigma_n^2 + \sigma^2)} \Re \left(\gamma_{ij} \int_{-\infty}^{\infty} y_{ij}^*(t) \frac{\partial u_i}{\partial \tau_{ij}} e^{j2\pi f_{D_{ij}}(t-\tau_{ij})} dt \right). \tag{A.2}$$

From here onwards we omit the argument of $u_i(t-\tau_{ij})$, to reduce space. The second derivative with respect to τ_{ij} is

$$\frac{\partial^2\Gamma_{ij}}{\partial\tau_{ij}^2} = \frac{\sigma^2}{2(\sigma_n^2+\sigma^2)}\left\{\Re\left(\int_{-\infty}^{\infty} y_{ij}(t)\overset{*}{u}_i(t-\tau_{ij})e^{-j2\pi f_{D_{ij}}(t-\tau_{ij})}dt\left(\int_{-\infty}^{\infty}\overset{*}{y}_{ij}(t)\frac{\partial^2 u_i}{\partial\tau_{ij}^2}e^{j2\pi f_{D_{ij}}(t-\tau_{ij})}dt\right.\right.\right.$$
$$\left.\left.\left. - j2\pi f_D\int_{-\infty}^{\infty}\overset{*}{y}_{ij}(t)\frac{\partial u_i}{\partial\tau_{ij}}e^{j2\pi f_{D_{ij}}(t-\tau_{ij})}dt\right) + \int_{-\infty}^{\infty}\overset{*}{y}_{ij}(t)\frac{\partial u_i}{\partial\tau_{ij}}e^{j2\pi f_{D_{ij}}(t-\tau_{ij})}dt\right.\right.$$
$$\left.\left.\left(\int_{-\infty}^{\infty} y_{ij}(t)\frac{\partial\overset{*}{u}_i}{\partial\tau_{ij}}e^{-j2\pi f_{D_{ij}}(t-\tau_{ij})}dt + 2j\pi f_D\int_{-\infty}^{\infty} y_{ij}(t)\overset{*}{u}_i(t-\tau_{ij})e^{-j2\pi f_{D_{ij}}(t-\tau_{ij})}dtdt\right)\right\},$$

which after some simplifications becomes,

$$\frac{\partial^2\Gamma_{ij}}{\partial\tau_{ij}^2} = \frac{\sigma^2}{2(\sigma_n^2+\sigma^2)}\left\{\Re\left(\int_{-\infty}^{\infty} y_{ij}(t)\overset{*}{u}_i e^{-j2\pi f_{D_{ij}}(t-\tau_{ij})}dt\int_{-\infty}^{\infty}\overset{*}{y}_{ij}(t)\frac{\partial^2 u_i}{\partial\tau_{ij}^2}e^{j2\pi f_{D_{ij}}(t-\tau_{ij})}dt+\right.\right.$$
$$\left.\left.\int_{-\infty}^{\infty}\overset{*}{y}_{ij}(t)\frac{\partial u_i}{\partial\tau_{ij}}e^{j2\pi f_{D_{ij}}(t-\tau_{ij})}dt\int_{-\infty}^{\infty} y_{ij}(t)\frac{\partial\overset{*}{u}_i}{\partial\tau_{ij}}e^{-j2\pi f_{D_{ij}}(t-\tau_{ij})}dt\right\}. \tag{A.3}$$

Now we take the expectation value while replacing the received signal from $y_{ij}(t)$ and using $\mathbb{E}[|\beta_{ij}|^2] = \sigma^2 + m_{ij}^2$, we arrive at the following equation

$$-\mathbb{E}\left(\frac{\partial^2\Gamma_{ij}}{\partial\tau_{ij}^2}\right) = \frac{-2\sigma^2(\sigma^2+m_{ij}^2)}{(\sigma_n^2+\sigma^2)}\mathbb{E}\left\{\Re\left(|\int_{-\infty}^{\infty} u_i\frac{\partial\overset{*}{u}_i}{\partial\tau_{ij}}dt|^2 + \int_{-\infty}^{\infty}|u_i|^2dt\int_{-\infty}^{\infty}\overset{*}{u}_i\frac{\partial^2 u_i}{\partial\tau_{ij}^2}dt\right)\right\}. \tag{A.4}$$

Now the derivative of u_i, is an odd function therefore the integrand of the first integral is an odd function, which makes it zero. On the other hand, the second term can simplified into

$$\int_{-\infty}^{\infty} \overset{*}{u_i} \frac{\partial^2 u_i}{\partial \tau_{ij}^2} dt = \frac{1}{N^2} \sum_{k=0}^{N-1} \sum_{n=0}^{N-1} \overset{*}{c_{ik}} c_{in} \int_{-\infty}^{\infty} \overset{*}{h_i} \left(t - \tau_{ij} - kT - \frac{D}{2} \right) \frac{\partial^2 h_i \left(t - \tau_{ij} - nT - \frac{D}{2} \right)}{\partial \tau_{ij}^2} dt,$$

where we have used the normalization condition $\int_{-\infty}^{\infty} |u_i|^2 dt = 1$. By using the expectation condition in Eq. (2.2) and Eq. (2.9) we obtain

$$-\mathbb{E}\left(\frac{\partial^2 \Gamma_{ij}}{\partial \tau_{ij}^2} \right) = \frac{-2\sigma^2(\sigma^2 + m_{ij}^2)}{(\sigma_n^2 + \sigma^2)} \left\{ \int_{-\infty}^{\infty} \overset{*}{h_i}(t) \frac{\partial^2 h_i(t)}{\partial t^2} dt \right\}.$$

The term in the bracket is already evaluated in [9], hence we get

$$-\mathbb{E}\left(\frac{\partial^2 \Gamma_{ij}}{\partial \tau_{ij}^2} \right) = \frac{2\sigma^2(\sigma^2 + |m_{ij}|^2)}{3T^2 \sigma_n^2 (\sigma_n^2 + \sigma^2)} \Big(\pi^2 + 3\alpha^2(\pi^2 - 8) \Big).$$

Finally, we write the above expression in terms of the SNR

$$-\mathbb{E}\left(\frac{\partial^2 \Gamma_{ij}}{\partial \tau_{ij}^2} \right) = \frac{2(\Upsilon_{NLoS})^2(1 + 2\kappa_{ij})}{3T^2(1 + \Upsilon_{NLoS})} \Big(\pi^2 + 3\alpha^2(\pi^2 - 8) \Big), \tag{A.5}$$

using $\kappa_{ij} = |m_{ij}|/2\sigma^2$ and $\Upsilon_{NLoS} = \sigma^2/\sigma_n^2$. To compute the expectation with respect to other second-order derivatives, we follow the same procedure and

arrive at the following closed-form expression

$$-\mathbb{E}\left(\frac{\partial^2\Gamma_{ij}}{\partial f_{D_{ij}}^2}\right) = \frac{\pi^2 T^2(\Upsilon_{NLoS})^2(1+2\kappa_{ij})}{6\alpha(1+\Upsilon_{NLoS})}\Big(3+4\alpha(N^2-1)). \tag{A.6}$$

The off-diagonal terms turn out to be zero in agreement with the calculations in [9], i.e.,

$$-\mathbb{E}\left(\frac{\partial^2\Gamma_{ij}}{\partial\tau_{ij}f_{D_{ij}}}\right) = 0. \tag{A.7}$$

Following the same lines, we obtain the expectation of second-order derivatives of Π_{ij} terms. By using Eq. (2.16), the first-derivative of Π_{ij}, is given by

$$\frac{\partial\Pi_{ij}}{\partial\tau_{ij}} = \frac{2}{(\sigma_n^2+\sigma^2)}\Re\left(\int_{-\infty}^{\infty} m_{y_{ij}}\overset{*}{u}_i(t-\tau_{ij})e^{-j2\pi f_{D_{ij}}(t-\tau_{ij})}dt\int_{-\infty}^{\infty} m_{y_{ij}}^{*}\frac{\partial u_i}{\partial\tau_{ij}}e^{j2\pi f_{D_{ij}}(t-\tau_{ij})}dt\right), \tag{A.8}$$

Now we take double derivates of Π_{ij} w.r.t τ ,
let $A = \int_{-\infty}^{\infty} m_{y_{ij}}\overset{*}{u}_i(t-\tau_{ij})e^{-j2\pi f_{D_{ij}}(t-\tau_{ij})}dt$ and $B = \int_{-\infty}^{\infty} m_{y_{ij}}^{*}\frac{\partial u_i}{\partial\tau_{ij}}e^{j2\pi f_{D_{ij}}(t-\tau_{ij})}dt$

$$\frac{\partial^2\Pi_{ij}}{\partial\tau_{ij}^2} = \frac{2}{(\sigma_n^2+\sigma^2)}\left\{\Re\left(A\frac{\partial B}{\partial\tau_{ij}}+B\frac{\partial A}{\partial\tau_{ij}}\right)\right\},$$

where we calculate the main term in parts as follows

$$\frac{\partial^2 \Pi_{ij}}{\partial \tau_{ij}^2} = \frac{-2}{(\sigma_n^2+\sigma^2)} \Re\Bigg(A\Bigg(\int_{-\infty}^{\infty} m_{y_{ij}}^* \frac{\partial^2 u_i}{\partial \tau_{ij}^2} e^{j2\pi f_{D_{ij}}(t-\tau_{ij})} dt - j2\pi f_{D_{ij}} \int_{-\infty}^{\infty} m_{y_{ij}}^* \frac{\partial u_i}{\partial \tau_{ij}} e^{j2\pi f_{D_{ij}}(t-\tau_{ij})} dt \Bigg) +$$
$$B\Bigg(\int_{-\infty}^{\infty} m_{y_{ij}} \frac{\partial \overset{*}{u}_i}{\partial \tau_{ij}} e^{-j2\pi f_{D_{ij}}(t-\tau_{ij})} dt + j2\pi f_{D_{ij}} \int_{-\infty}^{\infty} m_{y_{ij}} \overset{*}{u}_i(t-\tau_{ij}) e^{-j2\pi f_{D_{ij}}(t-\tau_{ij})} dt \Bigg)\Bigg).$$

$$\frac{\partial^2 \Pi_{ij}}{\partial \tau_{ij}^2} = \frac{-2}{(\sigma_n^2+\sigma^2)} \Re\Bigg(\int_{-\infty}^{\infty} m_{y_{ij}} \overset{*}{u}_i(t-\tau_{ij}) e^{-j2\pi f_{D_{ij}}(t-\tau_{ij})} dt \Bigg(\int_{-\infty}^{\infty} m_{y_{ij}}^* \frac{\partial^2 u_i}{\partial \tau_{ij}^2} e^{j2\pi f_{D_{ij}}(t-\tau_{ij})} dt +$$
$$\int_{-\infty}^{\infty} m_{y_{ij}}^* \frac{\partial u_i}{\partial \tau_{ij}} e^{j2\pi f_{D_{ij}}(t-\tau_{ij})} dt \Bigg(\int_{-\infty}^{\infty} m_{y_{ij}} \frac{\partial \overset{*}{u}_i}{\partial \tau_{ij}} e^{-j2\pi f_{D_{ij}}(t-\tau_{ij})} dt \Bigg)\Bigg)\Bigg).$$

this second derivative after taking the expectation takes the form

$$-\mathbb{E}\Bigg(\frac{\partial^2 \Pi_{ij}}{\partial \tau_{ij}^2}\Bigg) = \frac{-2}{(\sigma_n^2+\sigma^2)} \mathbb{E}\Bigg\{ \Re\Bigg(\int_{-\infty}^{\infty} m_{y_{ij}} \overset{*}{u}_i e^{-j2\pi f_{D_{ij}}(t-\tau_{ij})} dt \Bigg(\int_{-\infty}^{\infty} m_{y_{ij}}^* \frac{\partial^2 u_i}{\partial \tau_{ij}^2} e^{j2\pi f_{D_{ij}}(t-\tau_{ij})} dt +$$
$$\int_{-\infty}^{\infty} m_{y_{ij}}^* \frac{\partial u_i}{\partial \tau_{ij}} e^{j2\pi f_{D_{ij}}(t-\tau_{ij})} dt \Bigg(\int_{-\infty}^{\infty} m_{y_{ij}} \frac{\partial \overset{*}{u}_i}{\partial \tau_{ij}} e^{-j2\pi f_{D_{ij}}(t-\tau_{ij})} dt \Bigg)\Bigg)\Bigg)\Bigg\}. \tag{A.9}$$

Now after substituting the value of $m_{y_{ij}}$, i.e., $(m_{y_{ij}} = m_{ij} u_i\, e^{j2\pi f_{D_{ij}}(t-\tau_{ij})})$, and using the fact that the integral of an odd function is zero, it is easy to see that the second term in the above equation is zero while the first term

reduces to

$$-\mathbb{E}\left(\frac{\partial^2\Pi_{ij}}{\partial\tau_{ij}^2}\right) = \frac{-2|m_{ij}|^2}{(\sigma_n^2+\sigma^2)}\ \mathbb{E}\left\{\Re\left(\int_{-\infty}^{\infty} u_i^* \frac{\partial^2 u_i}{\partial\tau_{ij}^2} dt\right)\right\}, \tag{A.10}$$

which finally gives

$$-\mathbb{E}\left(\frac{\partial^2\Pi_{ij}}{\partial\tau_{ij}^2}\right) = \frac{2(\Upsilon_{NLoS})\kappa_{ij}}{3T^2(1+\Upsilon_{NLoS})}\Big(\pi^2+3\alpha^2(\pi^2-8)\Big). \tag{A.11}$$

Similarly the first derivative of Π_{ij}, with respect to $f_{D_{ij}}$ is

$$\frac{\partial\Pi_{ij}}{\partial f_{D_{ij}}} = \frac{2}{(\sigma_n^2+\sigma^2)}\Re\left(j2\pi\int_{-\infty}^{\infty} m_{y_{ij}} u_i^* e^{-j2\pi f_{D_{ij}}(t-\tau_{ij})}dt \times \int_{-\infty}^{\infty} m_{y_{ij}}^*(t-\tau_{ij}) u_i e^{j2\pi f_{D_{ij}}(t-\tau_{ij})}dt\right), \tag{A.12}$$

whereas the second derivative is

$$\frac{\partial^2\Pi_{ij}}{\partial f_{D_{ij}}^2} = \frac{2}{(\sigma_n^2+\sigma^2)}\ \Re\left(j2\pi\left(j2\pi\int_{-\infty}^{\infty} m_{y_{ij}} u_i^* e^{-j2\pi f_{D_{ij}}(t-\tau_{ij})}dt \int_{-\infty}^{\infty} m_{y_{ij}}^*(t-\tau)^2 u_i e^{j2\pi f_{D_{ij}}(t-\tau_{ij})}dt - \right.\right.$$
$$\left.\left. j2\pi\int_{-\infty}^{\infty}(t-\tau) m_{y_{ij}} u_i^* e^{-j2\pi f_{D_{ij}}(t-\tau_{ij})}dt \int_{-\infty}^{\infty} m_{y_{ij}}^*(t-\tau) u_i e^{j2\pi f_{D_{ij}}(t-\tau_{ij})}dt\right)\right)$$

which is simplified to

$$\frac{\partial^2 \Pi_{ij}}{\partial f_{D_{ij}}^2} = \frac{-8\pi^2}{(\sigma_n^2+\sigma^2)} \Re\Bigg(\int_{-\infty}^{\infty} m_{y_{ij}} \overset{*}{u_i} e^{-j2\pi f_{D_{ij}}(t-\tau_{ij})} dt \int_{-\infty}^{\infty} m^*_{y_{ij}}(t-\tau_{ij})^2 u_i e^{j2\pi f_{D_{ij}}(t-\tau_{ij})} dt -$$

$$- \int_{-\infty}^{\infty} m_{y_{ij}}(t-\tau_{ij}) \overset{*}{u_i} e^{-j2\pi f_{D_{ij}}(t-\tau_{ij})} dt \int_{-\infty}^{\infty} m^*_{y_{ij}}(t-\tau_{ij}) u_i e^{j2\pi f_{D_{ij}}(t-\tau_{ij})} dt \Bigg). \tag{A.13}$$

taking the expectation it becomes

$$- \mathbb{E}\left(\frac{\partial^2 \Pi_{ij}}{\partial f_{D_{ij}}^2}\right) = \frac{8\pi^2}{(\sigma_n^2+\sigma^2)} \mathbb{E}\Bigg\{ \Re\Bigg(\int_{-\infty}^{\infty} m_{y_{ij}} \overset{*}{u_i} e^{-j2\pi f_{D_{ij}}(t-\tau_{ij})} dt$$

$$\int_{-\infty}^{\infty} m^*_{y_{ij}}(t-\tau)^2 u_i e^{j2\pi f_{D_{ij}}(t-\tau_{ij})} dt -$$

$$\int_{-\infty}^{\infty} m_{y_{ij}}(t-\tau) \overset{*}{u_i} e^{-j2\pi f_{D_{ij}}(t-\tau_{ij})} dt \times \int_{-\infty}^{\infty} m^*_{y_{ij}}(t-\tau) u_i e^{j2\pi f_{D_{ij}}(t-\tau_{ij})} \Bigg) \Bigg\}$$

Now replacing mean as before, the above equation reduces to

$$-\mathbb{E}\left(\frac{\partial^2 \Pi_{ij}}{\partial f_{D_{ij}}^2}\right) = \frac{8\pi^2 |m_{ij}|^2}{(\sigma_n^2+\sigma^2)} \mathbb{E}\Bigg\{ \Re\Bigg(\int_{-\infty}^{\infty} (t-\tau_{ij})^2 |u_i|^2 dt - \int_{-\infty}^{\infty} (t-\tau_{ij}) |\overset{*}{u_i}|^2 dt \int_{-\infty}^{\infty} (t-\tau_{ij}) |u_i|^2 dt \Bigg) \Bigg\}. \tag{A.14}$$

Using the integration by parts we finally obtain

$$-\mathbb{E}\left(\frac{\partial^2\Pi_{ij}}{\partial f_{D_{ij}}^2}\right) = \frac{\pi^2 T^2(\Upsilon_{NLoS})\kappa_{ij}}{6\alpha(1+\Upsilon_{NLoS})}\Big(3+4\alpha(N^2-1)\Big).$$

The off-diagonal entries of the MFIM $\mathbf{F}^{\Pi}(\mathbf{\Phi})_{ij}$, are calculated as follows

$$-\mathbb{E}\left(\frac{\partial^2\Pi_{ij}}{\partial f_{D_{ij}}\partial\tau_{ij}}\right) = \frac{-4\pi}{(\sigma_n^2+\sigma^2)}\mathbb{E}\Bigg\{\Re\Bigg(j\Bigg(\int_{-\infty}^{\infty} m_{y_{ij}}u_i^* e^{-j2\pi f_{D_{ij}}(t-\tau_{ij})}dt \int_{-\infty}^{\infty} m_{y_{ij}}^*(t-\tau_{ij})$$
$$\frac{\partial u_i}{\partial\tau_{ij}}e^{j2\pi f_{D_{ij}}(t-\tau_{ij})}dt - \int_{-\infty}^{\infty} m_{y_{ij}}u_i^* e^{-j2\pi f_{D_{ij}}(t-\tau_{ij})}dt \int_{-\infty}^{\infty} m_{y_{ij}}^* u_i e^{j2\pi f_{D_{ij}}(t-\tau_{ij})}dt +$$
$$\int_{-\infty}^{\infty} m_{y_{ij}}^*(t-\tau_{ij})u_i e^{j2\pi f_{D_{ij}}}dt \int_{-\infty}^{\infty} m_{y_{ij}}\frac{\partial u_i^*}{\partial\tau_{ij}}e^{-j2\pi f_{D_{ij}}(t-\tau_{ij})}dt\Bigg)\Bigg)\Bigg\}, \tag{A.15}$$

which upon substituting the values of mean reduces to

$$-\mathbb{E}\left(\frac{\partial^2\Pi_{ij}}{\partial f_{D_{ij}}\partial\tau_{ij}}\right) = \frac{-4\pi}{(\sigma_n^2+\sigma^2)}\mathbb{E}\left\{\Re\left(j\left(\int_{-\infty}^{\infty}(t-\tau_{ij})u_i^*\frac{\partial u_i}{\partial\tau_{ij}}dt\right)\right\} = 0. \tag{A.16}$$

In order to calculate the MFIM, $\mathbf{F}^{\Sigma}(\mathbf{\Phi})_{ij}$, we have

$$\Sigma_{ij} = \frac{2}{(\sigma_n^2 + \sigma^2)} \Re\left(\int_{-\infty}^{\infty} y_{ij}(t) \dot{u}_i^* e^{-j2\pi f_{D_{ij}}(t-\tau_{ij})} dt \int_{-\infty}^{\infty} m_{y_{ij}}^* u_i e^{j2\pi f_{D_{ij}}(t-\tau_{ij})} dt \right), \tag{A.17}$$

which gives

$$\frac{\partial \Sigma_{ij}}{\partial \tau_{ij}} = \frac{2}{(\sigma_n^2 + \sigma^2)} \Re\left(\int_{-\infty}^{\infty} y_{ij}(t) \dot{u}_i^* e^{-j2\pi f_{D_{ij}}(t-\tau_{ij})} dt \int_{-\infty}^{\infty} m_{y_{ij}}^* \frac{\partial u_i}{\partial \tau_{ij}} e^{j2\pi f_{D_{ij}}(t-\tau_{ij})} dt + \right.$$

$$\left. \int_{-\infty}^{\infty} m_{y_{ij}}^* u_i e^{j2\pi f_{D_{ij}}(t-\tau_{ij})} dt \int_{-\infty}^{\infty} y_{ij}(t) \frac{\partial \dot{u}_i^*}{\partial \tau_{ij}} e^{-j2\pi f_{D_{ij}}(t-\tau_{ij})} dt \right). \tag{A.18}$$

Now to calculate the second derivative Let

$$\mathrm{I} = \int_{-\infty}^{\infty} y(t) \dot{u}_i^* e^{-j2\pi f_{D_{ij}}(t-\tau_{ij})} dt,$$

$$\mathrm{II} = \int_{-\infty}^{\infty} m_{y_{ij}}^* \frac{\partial u_i}{\partial \tau_{ij}} e^{j2\pi f_{D_{ij}}(t-\tau_{ij})} dt$$

$$\mathrm{III} = \int_{-\infty}^{\infty} m_{y_{ij}}^* u_i e^{j2\pi f_{D_{ij}}(t-\tau_{ij})} dt,$$

$$\mathrm{IV} = \int_{-\infty}^{\infty} y(t) \frac{\partial \dot{u}_i^*}{\partial \tau_{ij}} e^{-j2\pi f_{D_{ij}}(t-\tau_{ij})} dt$$

$$\frac{\partial^2 \Sigma_{ij}}{\partial \tau^2} = \frac{2}{(\sigma_n^2 + \sigma^2)} \Re\left(\mathrm{I}\frac{\partial \mathrm{II}}{\partial \tau} + \mathrm{II}\frac{\partial \mathrm{I}}{\partial \tau} + \mathrm{III}\frac{\partial \mathrm{IV}}{\partial \tau} + \mathrm{IV}\frac{\partial \mathrm{III}}{\partial \tau} \right)$$

where

$$\mathrm{I}\frac{\partial \mathrm{II}}{\partial \tau} = \int_{-\infty}^{\infty} y(t) \overset{*}{u}_i e^{-j2\pi f_{D_{ij}}(t-\tau_{ij})} dt \left(\int_{-\infty}^{\infty} \overset{*}{m}_{y_{ij}} \frac{\partial^2 u_i}{\partial \tau^2} e^{j2\pi f_{D_{ij}}(t-\tau_{ij})} dt \right.$$
$$\left. -j2\pi f_D \int_{-\infty}^{\infty} \overset{*}{m}_{y_{ij}} \frac{\partial u_i}{\partial \tau_{ij}} e^{j2\pi f_{D_{ij}}(t-\tau_{ij})} dt \right)$$

$$\mathrm{II}\frac{\partial \mathrm{I}}{\partial \tau} = \int_{-\infty}^{\infty} \frac{\partial \overset{*}{m}_{y_{ij}} u_i}{\partial \tau_{ij}} e^{j2\pi f_{D_{ij}}(t-\tau_{ij})} dt \left(\int_{-\infty}^{\infty} y(t) \frac{\partial \overset{*}{u}_i}{\partial \tau_{ij}} e^{-j2\pi f_{D_{ij}}(t-\tau_{ij})} dt \right.$$
$$\left. +j2\pi f_D \int_{-\infty}^{\infty} y(t) \overset{*}{u}_i e^{-j2\pi f_{D_{ij}}(t-\tau_{ij})} dt \right)$$

$$\mathrm{III}\frac{\partial \mathrm{IV}}{\partial \tau} = \int_{-\infty}^{\infty} \overset{*}{m}_{y_{ij}} u_i e^{j2\pi f_{D_{ij}}(t-\tau_{ij})} dt \left(\int_{-\infty}^{\infty} y(t) \frac{\partial^2 \overset{*}{u}_i}{\partial^2 \tau} e^{-j2\pi f_{D_{ij}}(t-\tau_{ij})} dt \right.$$
$$\left. +j2\pi f_D \int_{-\infty}^{\infty} y(t) \frac{\partial \overset{*}{u}_i}{\partial \tau} e^{-j2\pi f_{D_{ij}}(t-\tau_{ij})} dt \right)$$

$$\mathrm{IV}\frac{\partial \mathrm{III}}{\partial \tau} = \int_{-\infty}^{\infty} y(t)\frac{\partial u_i^*}{\partial \tau_{ij}} e^{-j2\pi f_{D_{ij}}(t-\tau_{ij})} dt \left(\int_{-\infty}^{\infty} m_{y_{ij}}^* \frac{\partial u_i}{\partial \tau_{ij}} e^{j2\pi f_{D_{ij}}(t-\tau_{ij})} dt \right.$$
$$\left. -j2\pi f_D \int_{-\infty}^{\infty} m_{y_{ij}}^* u_i e^{j2\pi f_{D_{ij}}(t-\tau_{ij})} dt \right)$$

Thus

$$\frac{\partial^2 \Sigma_{ij}}{\partial \tau^2} = \frac{2}{(\sigma_n^2+\sigma^2)} \Re\left(\int_{-\infty}^{\infty} y(t) u_i^* e^{-j2\pi f_{D_{ij}}(t-\tau_{ij})} dt \int_{-\infty}^{\infty} m_{y_{ij}}^* \frac{\partial^2 u_i}{\partial \tau^2} e^{j2\pi f_{D_{ij}}(t-\tau_{ij})} dt + \right.$$
$$\int_{-\infty}^{\infty} m_{y_{ij}}^* u_i e^{j2\pi f_{D_{ij}}(t-\tau_{ij})} dt \int_{-\infty}^{\infty} y(t) \frac{\partial^2 u_i^*}{\partial^2 \tau} e^{-j2\pi f_{D_{ij}}(t-\tau_{ij})} dt +$$
$$\left. 2\int_{-\infty}^{\infty} y(t)\frac{\partial u_i^*}{\partial \tau_{ij}} e^{-j2\pi f_{D_{ij}}(t-\tau_{ij})} dt \int_{-\infty}^{\infty} m_{y_{ij}}^* \frac{\partial u_i}{\partial \tau_{ij}} e^{j2\pi f_{D_{ij}}(t-\tau_{ij})} dt \right)$$

Subsequently, the second derivative becomes

$$\frac{\partial^2 \Sigma_{ij}}{\partial \tau_{ij}^2} = \frac{2}{(\sigma_n^2+\sigma^2)} \Re\left(\left(\int_{-\infty}^{\infty} y_{ij}(t) u_i^* e^{-j2\pi f_{D_{ij}}(t-\tau_{ij})} dt \int_{-\infty}^{\infty} m_{y_{ij}}^* \frac{\partial^2 u_i}{\partial \tau_{ij}^2} e^{j2\pi f_{D_{ij}}(t-\tau_{ij})} dt \right.\right.$$
$$+ \int_{-\infty}^{\infty} m_{y_{ij}}^* u_i e^{j2\pi f_{D_{ij}}(t-\tau_{ij})} dt \times \int_{-\infty}^{\infty} y_{ij}(t) \frac{\partial^2 u_i^*}{\partial \tau_{ij}^2} e^{-j2\pi f_{D_{ij}}(t-\tau_{ij})} dt -$$
$$\left.\left. 2\int_{-\infty}^{\infty} y_{ij}(t)\frac{\partial u_i^*}{\partial \tau_{ij}} e^{-j2\pi f_{D_{ij}}(t-\tau_{ij})} dt \int_{-\infty}^{\infty} m_{y_{ij}}^* \frac{\partial u_i}{\partial \tau_{ij}} e^{j2\pi f_{D_{ij}}(t-\tau_{ij})} dt \right) \right). \tag{A.19}$$

Thus we have

$$-\mathbb{E}\left(\frac{\partial^2\Sigma_{ij}}{\partial\tau_{ij}^2}\right) = \frac{-2}{(\sigma_n^2+\sigma^2)}\mathbb{E}\Bigg\{\Re\Bigg(\int_{-\infty}^{\infty}|u_i|^2dt\int_{-\infty}^{\infty}m_{y_{ij}}^*\frac{\partial^2u_i}{\partial\tau_{ij}^2}e^{j2\pi f_{D_{ij}}(t-\tau_{ij})}dt+$$

$$\int_{-\infty}^{\infty}m_{y_{ij}}^*u_ie^{j2\pi f_{D_{ij}}(t-\tau_{ij})}dt\int_{-\infty}^{\infty}u_i\frac{\partial^2u_i^*}{\partial\tau_{ij}^2}dt+2\int_{-\infty}^{\infty}u_i\frac{\partial u_i^*}{\partial\tau_{ij}}dt\int_{-\infty}^{\infty}m_{y_{ij}}^*\frac{\partial u_i}{\partial\tau_{ij}}e^{j2\pi f_{D_{ij}}(t-\tau_{ij})}dt\Bigg)\Bigg\}. \tag{A.20}$$

Now, putting value of $y_{ij}(t)$, mean $m_{y_{ij}}$ and using $\mathbb{E}\{|\beta_{ij}|^2\} = \sigma^2 + m_{ij}$, we obtain

$$-\mathbb{E}\left(\frac{\partial^2\Sigma_{ij}}{\partial\tau_{ij}^2}\right) = \frac{-2}{(\sigma_n^2+\sigma^2)}\ \mathbb{E}\Bigg\{\Re\Bigg(\int_{-\infty}^{\infty}2u_i^*\frac{\partial^2u_i}{\partial\tau_{ij}^2}dt\Bigg)\Bigg\}. \tag{A.21}$$

Lastly, we obtain a closed-form expression

$$-\mathbb{E}\left(\frac{\partial^2\Sigma_{ij}}{\partial\tau_{ij}^2}\right) = \frac{4(\Upsilon_{NLoS})\kappa_{ij}\Big(\pi^2+3\alpha^2(\pi^2-8)\Big)}{3T^2(1+\Upsilon_{NLoS})}. \tag{A.22}$$

Similarly the derivatives of Σ_{ij}, with respect to $f_{D_{ij}}$ is

$$\frac{\partial \Sigma_{ij}}{\partial f_{D_{ij}}} = \frac{2}{(\sigma_n^2+\sigma^2)} \Re\Bigg(j2\pi \Bigg(\int_{-\infty}^{\infty} y_{ij}(t) \hat{u}_i^* e^{-j2\pi f_{D_{ij}}(t-\tau_{ij})} dt \int_{-\infty}^{\infty} (t-\tau_{ij}) m_{y_{ij}}^* u_i e^{j2\pi f_{D_{ij}}(t-\tau_{ij})} dt - \int_{-\infty}^{\infty} (t-\tau_{ij}) y_{ij}(t) \hat{u}_i^* e^{-j2\pi f_{D_{ij}}(t-\tau_{ij})} dt \int_{-\infty}^{\infty} m_{y_{ij}}^* u_i e^{j2\pi f_{D_{ij}}(t-\tau_{ij})} dt \Bigg) \Bigg), \tag{A.23}$$

which gives

$$\begin{aligned} \frac{\partial^2 \Sigma_{ij}}{\partial f_{D_{ij}}^2} = \frac{2}{(\sigma_n^2+\sigma^2)} \Re\Bigg(-4\pi^2 \Bigg(& \int_{-\infty}^{\infty} y_{ij}(t) \hat{u}_i^* e^{-j2\pi f_{D_{ij}}(t-\tau_{ij})} dt \int_{-\infty}^{\infty} (t-\tau_{ij})^2 m_{y_{ij}}^* u_i e^{j2\pi f_{D_{ij}}(t-\tau_{ij})} dt \\ & + \int_{-\infty}^{\infty} (t-\tau_{ij})^2 y_{ij}(t) \hat{u}_i^* e^{-j2\pi f_{D_{ij}}(t-\tau_{ij})} dt \int_{-\infty}^{\infty} m_{y_{ij}}^* u_i e^{j2\pi f_{D_{ij}}(t-\tau_{ij})} dt - \\ & - 2 \int_{-\infty}^{\infty} (t-\tau_{ij}) y_{ij}(t) \hat{u}_i^* e^{-j2\pi f_{D_{ij}}(t-\tau_{ij})} dt \int_{-\infty}^{\infty} (t-\tau_{ij}) m_{y_{ij}}^* u_i e^{j2\pi f_{D_{ij}}(t-\tau_{ij})} dt \Bigg) \Bigg). \end{aligned} \tag{A.24}$$

Subsequently we get

$$-\mathbb{E}\left(\frac{\partial^2\Sigma_{ij}}{\partial f_{D_{ij}}^2}\right) = \frac{8\pi^2}{(\sigma_n^2+\sigma^2)}\mathbb{E}\Bigg\{\Re\Bigg(\int_{-\infty}^{\infty}|u_i|^2dt\int_{-\infty}^{\infty}m_{y_{ij}}^*(t-\tau_{ij})^2u_ie^{j2\pi f_{D_{ij}}(t-\tau_{ij})}dt + \int_{-\infty}^{\infty}(t-\tau_{ij})^2|u_i|^2dt\int_{-\infty}^{\infty}m_{y_{ij}}^*u_ie^{j2\pi f_{D_{ij}}(t-\tau_{ij})}dt - 2\int_{-\infty}^{\infty}(t-\tau_{ij})|u_i|^2dt\int_{-\infty}^{\infty}(t-\tau_{ij})m_{y_{ij}}^*u_ie^{j2\pi f_{D_{ij}}(t-\tau_{ij})}dt\Bigg)\Bigg\}. \tag{A.25}$$

Again after substituting the value of mean $m_{y_{ij}}$ as before we get

$$-\mathbb{E}\left(\frac{\partial^2\Sigma_{ij}}{\partial f_{D_{ij}}^2}\right) = \frac{16\pi^2}{(\sigma_n^2+\sigma^2)}\ \mathbb{E}\Bigg\{\Re\Bigg(\int_{-\infty}^{\infty}(t-\tau_{ij})^2|u_i|^2dt - \int_{-\infty}^{\infty}(t-\tau_{ij})|\dot{u}_i^*|^2\int_{-\infty}^{\infty}(t-\tau_{ij})|u_i|^2\Bigg)\Bigg\}. \tag{A.26}$$

Hence,

$$-\mathbb{E}\left(\frac{\partial^2\Sigma_{ij}}{\partial f_{D_{ij}}^2}\right) = \frac{\pi^2T^2(\Upsilon_{NLoS})\kappa_{ij}\Big(3+4\alpha(N^2-1)\Big)}{3\alpha(1+\Upsilon_{NLoS})}. \tag{A.27}$$

On the other hand, the off-diagonal terms of the MFIM, $\mathbf{F}^{\Sigma}(\mathbf{\Phi})_{ij}$, are calcu-

lated as follows

$$\frac{\partial \Sigma_{ij}}{\partial \tau_{ij}} = \frac{2}{(\sigma_n^2+\sigma^2)} \times$$
$$\Re\left(\left(\int_{-\infty}^{\infty} m^*_{y_{ij}} y_{ij}(t) u_i^* e^{-j2\pi f_{D_{ij}}(t-\tau_{ij})} dt \times \int_{-\infty}^{\infty} \frac{\partial u_i}{\partial \tau_{ij}} e^{j2\pi f_{D_{ij}}(t-\tau_{ij})} dt \right.\right.$$
$$\left.\left. + \int_{-\infty}^{\infty} u_i e^{j2\pi f_{D_{ij}}(t-\tau_{ij})} dt \int_{-\infty}^{\infty} \frac{\partial u_i^*}{\partial \tau_{ij}} e^{-j2\pi f_{D_{ij}}(t-\tau_{ij})} dt \right)\right), \tag{A.28}$$

which implies after simplification

$$-\mathbb{E}\left(\frac{\partial^2 \Sigma_{ij}}{\partial f_{D_{ij}} \partial \tau_{ij}}\right) = \frac{-4\pi}{(\sigma_n^2+\sigma^2)} \mathbb{E}\left\{\Re\left(j\left(\int_{-\infty}^{\infty} |u_i|^2 dt \int_{-\infty}^{\infty} m^*_{y_{ij}}(t-\tau_{ij}) \frac{\partial u_i}{\partial \tau_{ij}} e^{j2\pi f_{D_{ij}}(t-\tau_{ij})} dt - \right.\right.\right.$$
$$\int_{-\infty}^{\infty} (t-\tau_{ij}) |u_i|^2 dt \int_{-\infty}^{\infty} m^*_{y_{ij}} \frac{\partial u_i}{\partial \tau_{ij}} e^{j2\pi f_{D_{ij}}(t-\tau_{ij})} dt -$$
$$\left.\left.\left. \int_{-\infty}^{\infty} (t-\tau_{ij}) u_i \frac{\partial u_i^*}{\partial \tau_{ij}} dt \int_{-\infty}^{\infty} m^*_{y_{ij}} u_i e^{j2\pi f_{D_{ij}}(t-\tau_{ij})} dt + \int_{-\infty}^{\infty} u_i \frac{\partial u_i^*}{\partial \tau_{ij}} dt \int_{-\infty}^{\infty} m^*_{y_{ij}}(t-\tau_{ij}) u_i e^{j2\pi f_{D_{ij}}(t-\tau_{ij})} dt \right)\right)\right\}$$

(A.29)

Therefore, by putting the value of $y_{ij}(t)$ and using $\mathbb{E}\{\beta_{ij}\} = m_{ij}$, we have

$$-\mathbb{E}\left(\frac{\partial^2\Sigma_{ij}}{\partial f_{D_{ij}}\partial\tau_{ij}}\right) = \frac{-4\pi}{(\sigma_n^2+\sigma^2)}\mathbb{E}\Bigg\{\Re\Bigg(j\Bigg(\int_{-\infty}^{\infty} u_i^* \frac{\partial u_i}{\partial\tau_{ij}}dt - \int_{-\infty}^{\infty}(t-\tau_{ij})|u_i|^2 dt \int_{-\infty}^{\infty} u_i^* \frac{\partial u_i}{\partial\tau_{ij}}dt -$$
$$\int_{-\infty}^{\infty}(t-\tau_{ij})u_i\frac{\partial u_i^*}{\partial\tau_{ij}}dt + \int_{-\infty}^{\infty} u\frac{\partial u_i^*}{\partial\tau_{ij}}dt\Bigg)\Bigg)\Bigg\} = 0 \qquad \text{(A.30)}$$

which ends the proof of Theorem 1.

A.1 Entries of MFIM

The Entries of MFIM $\mathbf{F}_{ij}(\boldsymbol{\Theta})$

As is clear that the required MFIM $\mathbf{F}_{ij}(\boldsymbol{\Theta})$, is a 6×6 symmetric matrix which arises on the parameters of interest and it depends more on the geometry due to presence of the Jacobian rather than $\mathbf{F}_{ij}(\boldsymbol{\Phi})$. Since the MFIM on parameter, $\Phi = [\tau_{ij}, f_{D_{ij}}]$ is only a diagonal matrix of order 2×2, we denote it by $\mathbf{F}_{ij}(\boldsymbol{\Phi}) = \text{diag}[F^{11}, F^{22}]$, thus all entries of the required MFIM are

explicitly given subsequently.

$$\mathbf{F}_{ij}^{11}(\mathbf{\Theta}) = (\tau_{ij\,,p_x})^2 F^{11} + (f_{D_{ij,p_x}})^2 F^{22},$$

$$\mathbf{F}_{ij}^{12}(\mathbf{\Theta}) = (\tau_{ij\,,p_x})(\tau_{ij\,,p_y}) F^{11} + (f_{D_{ij,p_x}})(f_{D_{ij,p_y}}) F^{22},$$

$$\mathbf{F}_{ij}^{13}(\mathbf{\Theta}) = (\tau_{ij\,,p_x})(\tau_{ij\,,p_z}) F^{11} + (f_{D_{ij,p_x}})(f_{D_{ij,p_z}}) F^{22},$$

$$\mathbf{F}_{ij}^{14}(\mathbf{\Theta}) = (f_{D_{ij,p_x}})(f_{D_{ij,v_x}}) F^{22},$$

$$\mathbf{F}_{ij}^{15}(\mathbf{\Theta}) = (f_{D_{ij,p_x}})(f_{D_{ij,v_y}}) F^{22},$$

$$\mathbf{F}_{ij}^{16}(\mathbf{\Theta}) = (f_{D_{ij,p_x}})(f_{D_{ij,v_z}}) F^{22},$$

$$\mathbf{F}_{ij}^{22}(\mathbf{\Theta}) = (\tau_{ij\,,p_y})^2 F^{11} + (f_{D_{ij,p_y}})^2 F^{22},$$

$$\mathbf{F}_{ij}^{23}(\mathbf{\Theta}) = (\tau_{ij\,,p_y})(\tau_{ij\,,p_z}) F^{11} + (f_{D_{ij,p_y}})(f_{D_{ij,p_z}}) F^{22},$$

$$\mathbf{F}_{ij}^{24}(\mathbf{\Theta}) = (f_{D_{ij,p_y}})(f_{D_{ij,v_x}}) F^{22},$$

$$\mathbf{F}_{ij}^{25}(\mathbf{\Theta}) = (f_{D_{ij,p_y}})(f_{D_{ij,v_y}}) F^{22},$$

$$\mathbf{F}_{ij}^{26}(\mathbf{\Theta}) = (f_{D_{ij,p_y}})(f_{D_{ij,v_z}}) F^{22},$$

$$\mathbf{F}_{ij}^{33}(\mathbf{\Theta}) = (\tau_{ij}, p_z)^2 F^{11} + (f_{D_{ij,p_z}})^2 F^{22},$$

$$\mathbf{F}_{ij}^{34}(\mathbf{\Theta}) = (f_{D_{ij,p_z}})(f_{D_{ij,v_x}}) F^{22},$$

$$\mathbf{F}_{ij}^{35}(\mathbf{\Theta}) = (f_{D_{ij,p_z}})(f_{D_{ij,v_y}}) F^{22},$$

$$\mathbf{F}_{ij}^{36}(\mathbf{\Theta}) = (f_{D_{ij,p_z}})(f_{D_{ij,v_z}}) F^{22},$$

$$\mathbf{F}_{ij}^{44}(\mathbf{\Theta}) = (f_{D_{ij,v_x}})^2 F^{22},$$

$$\mathbf{F}_{ij}^{45}(\mathbf{\Theta}) = (f_{D_{ij,v_x}})(f_{D_{ij,v_y}}) F^{22},$$

$$\mathbf{F}_{ij}^{46}(\mathbf{\Theta}) = (f_{ij,v_x})(f_{ij,v_z}) F^{22},$$

$$\mathbf{F}_{ij}^{55}(\mathbf{\Theta}) = (f_{D_{ij,v_y}})^2 F^{22},$$

$$\mathbf{F}_{ij}^{56}(\mathbf{\Theta}) = (f_{D_{ij,v_y}})(f_{D_{ij,v_z}}) F^{22},$$

$$\mathbf{F}_{ij}^{66}(\mathbf{\Theta}) = (f_{D_{ij,v_z}})^2 F^{22}.$$

A.2 Proof of Lemma 2

Proof of Lemma 2.

In order to prove the positive definiteness of the Schur complement we first identify the centers of the Gershgorin discs in it and show that these are positive. Again by using the results in Appendix 2, the explicit form of the diagonal entries of $\mathbf{\Omega^{2}}^{T}\mathbf{\Omega^{3}}^{-1}\mathbf{\Omega^{2}}$, are given by

$$\operatorname{diag}\left(\mathbf{\Omega^{2}}^{T}\mathbf{\Omega^{3}}^{-1}\mathbf{\Omega^{2}}\right) = \left(F^{22}\right)^{2}\begin{bmatrix}\omega_1 s_1^2+\omega_4 s_2^2+\omega_6 s_3^2+2(\omega_3 s_1 s_3+\omega_5 s_2 s_3+\omega_2 s_1 s_2)\\ \omega_1 s_2^2+\omega_4 s_4^2+\omega_6 s_5^2+2(\omega_3 s_2 s_5+\omega_5 s_4 s_5+\omega_2 s_2 s_4)\\ \omega_1 s_3^2+\omega_4 s_5^2+\omega_6 s_6^2+2(\omega_3 s_3 s_6+\omega_5 s_5 s_6+\omega_2 s_3 s_5)\end{bmatrix}, \tag{A.31}$$

where we have used the fact that $\mathbf{\Omega^{2}}^{T} = \mathbf{\Omega^{2}}$. Here ω_i for all $i = 1, ..., 6$ denote the entries of the inverse matrix $\mathbf{\Omega^{3}}^{-1}$ and s_i for all $i = 1, ..., 6$ denote the matrix $\mathbf{\Omega^{2}}$ and identified as

$$s_1 = \sum_{i,j} f_{D_{ij,p_x}} f_{D_{ij,v_x}},\ s_2 = \sum_{i,j} f_{D_{ij,p_x}} f_{D_{ij,v_y}}, s_3 = \sum_{i,j} f_{D_{ij,p_x}} f_{ij,v_z}, \tag{A.32}$$

$$s_4 = \sum_{i,j} f_{D_{ij,p_y}} f_{D_{ij,v_y}},\ s_5 = \sum_{i,j} f_{D_{ij,p_y}} f_{D_{ij,v_z}},\ s_6 = \sum_{i,j} f_{D_{ij,p_z}} f_{D_{ij,v_z}}. \tag{A.33}$$

Following the same lines the entries of inverse matrix $\mathbf{\Omega^{3}}^{-1}$, are determined

as

$$\tilde{D}\omega_1 = \sum_{i,j} \tilde{\kappa}_{ij} f^2_{Dij,v_y} \sum_{i,j} \tilde{\kappa}_{ij} f^2_{Dij,v_z} - \left(\sum_{i,j} \tilde{\kappa}_{ij} f_{Dij,v_y} f_{Dij,v_z} \right)^2, \tag{A.34}$$

$$\tilde{D}\omega_2 = \sum_{i,j} \tilde{\kappa}_{ij} f_{ij,v_x} f_{Dij,v_z} \sum_{i,j} \tilde{\kappa}_{ij} f^2_{Dij,v_y} - \sum_{i,j} \tilde{\kappa}_{ij} f_{Dij,v_x} f_{Dij,v_y} \sum_{i,j} \tilde{\kappa}_{ij} f^2_{Dij,v_z}, \tag{A.35}$$

$$\tilde{D}\omega_3 = \sum_{i,j} \tilde{\kappa}_{ij} f_{Dij,v_x} f_{Dij,v_y} \sum_{i,j} \tilde{\kappa}_{ij} f_{Dij,v_y} f_{Dij,v_z} - \sum_{i,j} \tilde{\kappa}_{ij} f_{ij,v_x} f_{Dij,v_z} \sum_{i,j} \tilde{\kappa}_{ij} f^2_{Dij,v_y}, \tag{A.36}$$

$$\tilde{D}\omega_4 = \sum_{i,j} \tilde{\kappa}_{ij} f^2_{Dij,v_x} \sum_{i,j} \tilde{\kappa}_{ij} f^2_{Dij,v_z} - \left(\sum_{i,j} \tilde{\kappa}_{ij} f_{ij,v_x} f_{Dij,v_z} \right)^2, \tag{A.37}$$

$$\tilde{D}\omega_5 = \sum_{i,j} \tilde{\kappa}_{ij} f_{Dij,v_x} f_{Dij,v_y} \sum_{i,j} \tilde{\kappa}_{ij} f_{ij,v_x} f_{Dij,v_z} - \sum_{i,j} \tilde{\kappa}_{ij} f^2_{Dij,v_x} \sum_{i,j} \tilde{\kappa}_{ij} f_{Dij,v_y} f_{Dij,v_z}, \tag{A.38}$$

$$\tilde{D}\omega_6 = \sum_{i,j} \tilde{\kappa}_{ij} f^2_{Dij,v_x} \sum_{i,j} \tilde{\kappa}_{ij} f^2_{Dij,v_y} - \left(\sum_{i,j} \tilde{\kappa}_{ij} f_{Dij,v_x} f_{Dij,v_y} \right)^2, \tag{A.39}$$

where $\tilde{D} = \mathrm{Det}(\mathbf{\Omega^3})$. Now by substituting these values in the Eq. (A.31) and observing that each entry is the sum of several terms in which the first three terms are positive following the inequality (3.24) in Lemma 1. It is easy to see that the first three terms in each diagonal entry are dominating which implies that each such diagonal entry is positive. Hence the center of each Gershgorin disc is situated at a positive real number which in turn indicate that the Schur complement is also positive definite which completes the proof of Lemma 2.

Bibliography

[1] H. D. Griffiths, "New directions in bistatic radar," *IEEE Radar conf. (RADAR)*, pp. 1–6, 2008.

[2] Nicholas J. Willis, *Bistatic radar.*, SciTech Publishing, 2005.

[3] H. D. Griffiths, and C. J. Baker, "Passive coherent location radar systems. Part 1: performance prediction," *IET Radar, Sonar & Navigation*, Vol. 152. no. 3. pp. 153–159, 2005.

[4] L. Neng-Jing, "Radar ECCMS new area: anti-stealth and anti-ARM," *IEEE Trans. Aerospace and Electronic Systems*, vol. 31, no. 3, pp. 1120-1127, 1995.

[5] H. Griffiths, "Passive bistatic radar and waveform diversity," Tech. Rep., *DTIC Document*, 2009.

[6] Chetty, Kevin, E. Smith Graeme , and Karl Woodbridge, "Through-the-wall sensing of personnel using passive bistatic wifi radar at standoff distances," *IEEE Transactions on Geoscience and Remote Sensing*, pp. 1218–122, vol. 50, 2012.

[7] Tsu-Chin Tsao, Mustapha Slamani, Praveen Varshney, D. Weiner, and H. Schwarzlander, "Ambiguity function for a bistatic radar," *IEEE Trans. Aerospace and Electronic Systems*, pp. 1041–1051, vol. 3, 1997.

[8] M. C. Jackson, "The geometry of bistatic radar systems," *IEE Proceedings on Communications, Radar and Signal Processing,* pp. 604–612, vol. 33, 1986.

[9] P. Stinco, M. S. Greco, F. Gini, and M. Rangaswamy, "Ambiguity function and Cramer-Rao bounds for universal mobile telecommunications system-based passive coherent location systems," *IET Radar, Sonar & Navigation*, vol. 6, no. 7, pp. 668-678, 2012.

[10] M. Malanowski, K. Kulpa, J. Kulpa, P. Samczynski, and J. Misiurewicz, "Analysis of detection range of FM-based passive radar," *IET Radar, Sonar & Navigation*, vol. 8, no. 2, pp. 153-159, 2014.

[11] Plsek, Radek, Vojtech Stejskal, Martin Pelant, and Martin Vojacek, "FM based passive coherent radar: From detections to tracks," *Tyrrhenian International Workshop on Digital Communications-Enhanced Surveillance of Aircraft and Vehicles*, 2011.

[12] Paul E. Howland, D. Maksimiuk, and G. Reitsma, "FM radio based bistatic radar," *IEE Proceedings-Radar, Sonar and Navigation*, pp. 107–115, vol. 152, 2005.

[13] A. Farina, R. Fulcoli, P. Genovesi, R. Lalli, and R. Mancinelli, "Design, development and test on real data of an FM based prototypical passive radar," *IEEE Radar conf. (RADAR)*, pp. 1–6, 2008.

[14] C. Coleman and H. Yardley, "Passive bistatic radar based on target illuminations by digital audio broadcasting," *IET Radar, Sonar & Navigation*, vol. 2, no. 5, pp. 366-375, 2008.

[15] C. Coleman, R. Watson, and H. Yardley, "A practical bistatic passive radar system for use with DAB and DRM illuminators," *IEEE Radar conf. (RADAR)*, 2008.

[16] Heath J. Yardley, "Bistatic radar based on DAB illuminators: the evolution of a practical system," *IEEE Radar conf. (RADAR)*, pp. 688–692, 2007.

[17] M. Radmard, M. Bastani, F. Behnia, and M. M. Nayebi, "Cross ambiguity function analysis of the '8k-mode' DVB-T for passive radar application," *IEEE International Radar Symposium (IRS)*, pp. 1-4, 2010.

[18] H. Harms, Linda Andrew, M. Davis, and James Palmer, "Understanding the signal structure in DVB-T signals for passive radar detection," *IEEE Radar conf. (RADAR)*, pp. 532–537, 2010.

[19] D. Langellotti, F. Colone, P. Lombardo, E. Tilli, M. Sedehi, and A. Farina, "Over the horizon maritime surveillance capability of DVB-T based passive radar," *IEEE European Radar Conference (EuRAD)*, pp. 509-512, 2014.

[20] Danny KP Tan, Hongbo Sun, Yilong Lu, and Weixian Liu, "Feasibility analysis of GSM signal for passive radar," *IEEE Radar conf. (RADAR)*, pp. 425–430, 2003.

[21] P. Samczynski, , K. Kulpa, M. Malanowski, P. Krysik, and L. MaÅŻlikowski, "A concept of GSM-based passive radar for vehicle traffic monitoring," *IEEE Microwaves, Radar and Remote Sensing Symposium (MRRS)*, pp. 271–274, 2011.

[22] Hongbo Sun, Danny KP Tan, Yllong Lu, and Marc Lesturgie, "Applications of passive surveillance radar system using cell phone base station illuminators," *IEEE Aerospace and Electronic Systems Magazine,* pp. 10–18, vol. 25, 2010.

[23] D. Petri, Amerigo Capria, Marco Martorella, and Fabrizio Berizzi, "Ambiguity function study for UMTS passive radar," *IEEE European Radar Conference (EuRAD)*, pp. 41–44, 2009.

[24] S. Gogineni, M. Rangaswamy, B. D. Rigling, and A. Nehorai, "Ambiguity function analysis for UMTS-based passive multistatic radar," *IEEE Trans. Signal Processing*, vol. 62, no. 11, pp. 2945-2957, 2014.

[25] D. Petri, F. Berizzi, M. Martorella, E. Dalle Mese, and A. Capria, "A software defined UMTS passive radar demonstrator." *IEEE International Radar Symposium (IRS)*, pp. 1–4, 2010.

[26] P. Stinco, M. S. Greco, and F. Gini, "White space passive coherent location system based on IEEE 802.22," *IEEE International Radar Symposium (IRS)*, pp. 71-76, 2015.

[27] M. Malanowski, K. Kulpa, J. Kulpa, P. Samczynski, and J. Misiurewicz, "Analysis of detection range of FM-based passive radar," *IET Radar, Sonar & Navigation*, vol. 8, no. 2, pp. 153-159, 2014.

[28] C. Coleman and H. Yardley, "Passive bistatic radar based on target illuminations by digital audio broadcasting," *IET Radar, Sonar & Navigation*, vol. 2, no. 5, pp. 366-375, 2008.

[29] M. Wielgo, P. Krysik, K. Klincewicz, L. Maslikowski, S. Rzewuski, and K.Kulpa, "Doppler only localization in GSM-based passive radar," *IEEE. International Radar Conference (RadarCon)*, pp. 1–6. 2014.

[30] A. Capria, D. Petri, C. Moscardini, et. al, "Software-defined Multiband Array Passive Radar (SMARP) demonstrator: A test and evaluation perspective," *IEEE. OCEANS Genova*, pp. 1–6, 2015.

[31] A. Evers and J. A. Jackson, "Analysis of an LTE waveform for radar applications," *IEEE Radar conf. (RADAR)*, pp. 200-205, 2014.

[32] Stefania Bartoletti, Andrea Conti, and Moe Z. Win, "Passive radar via LTE signals of opportunity," *IEEE Communications Workshops (ICC)*, pp. 181–185. 2014.

[33] Aaron Evers, and Joana Abreu Jackson, ""Experimental passive SAR imaging exploiting LTE, DVB, and DAB signals," *IEEE. International Radar Conference (RadarCon)*, pp. 0680–0685, 2014.

[34] H.Guo, K. Woodbridge, and C. J. Baker, "Evaluation of WiFi beacon transmissions for wireless based passive radar." *IEEE. International Radar Conference (RadarCon)*, pp. 1–6. IEEE, 2008.

[35] Chetty, Graeme Smith, Hui Guo, and Karl Woodbridge, "Target detection in high clutter using passive bistatic WiFi radar," *IEEE. International Radar Conference (RadarCon)*, pp. 1–5, 2009.

[36] Q. Wang, C. Hou, and Y. Lu, "An experimental study of WIMAX-based passive radar," *IEEE Trans. Microwave Theory and Techniques*, vol. 58, no. 12, pp. 3502-3510, 2010.

[37] Chetty, Karl Woodbridge, Hui Guo, and Graeme E. Smith, "Passive bistatic WiMAX radar for marine surveillance," *IEEE. International Radar Conference (RadarCon)*, pp. 188–193. IEEE, 2010.

[38] "Technical Specifications Group Radio Access Network;Spreading and modulation (FDD)," Std.TS 25.213, *3rd Generation Partnership Project (3GPP)*, 2006.

[39] B. H. Walke, P. Seidenberg, and M. P. Althoff, *UMTS: The Fundamentals*, John Wiley & Sons, 2003.

[40] A. De Maio, G. Foglia, N. Pasquino, and M. Vadursi, "Measurement and comparative analysis of clutter for GSM and UMTS passive radars," *IET Radar, Sonar & Navigation*, vol. 4, no. 3, pp. 412-423, 2010.

[41] S. Gogineni, M. Rangaswamy, B. D. Rigling, and A. Nehorai, "Cramér-Rao bounds for UMTS-based passive multistatic radar," *IEEE Trans. Signal Processing*, vol. 62, no. 1, pp. 95–106, 2014.

[42] Q. He, R. S. Blum, and A. M. Haimovich, "Non-coherent MIMO radar for target estimation: More antennas means better performance," *IEEE Conf. Information Sciences and Systems (CISS)*, pp. 108-113, 2009.

[43] Anastasio, Valeria, Fabiola Colone, and Pierfrancesco Lombardo, "A procedure for effective receiver positioning in multistatic passive radar," *IEEE European Radar Conference (EuRAD)*, pp. 493–496, 2009.

[44] Greco, P. Stinco, F. Gini, A. Farina, and M. Rangaswamy, "Cramer-Rao bounds and TX-RX selection in a multistatic radar scenario," *IEEE. International Radar Conference (RadarCon)*, pp. 1371–1376, 2010.

[45] Anastasio, V., F. Colone, A. Di Lallo, A. Farina, F. Gumiero, and P. Lombardo, "Optimization of multistatic passive radar geometry based on CRLB with uncertain observations," *IEEE European Radar Conference (EuRAD)*, pp. 340–343, 2010.

[46] M. A. Richards, *Fundamentals of Radar Signal Processing.*, Tata McGraw-Hill Education, 2005.

[47] P. Swerling, "Probability of Detection for Fluctuating Targets," *IRE Trans. Information Theory*, vol. 6, no. 2, pp. 269-308, 1960

[48] I. S. Merrill, *Radar Handbook*, McGrawHill, NewYork, 1990.

[49] C. D. Papanicolopoulos, W. D. Blair, D. L. Sherman, and M. Brandt-Pearce, "Use of a Rician Distribution for Modeling Aspect-Dependent RCS Amplitude and Scintillation," *IEEE Radar conf. (RADAR)*, pp. 218–223, 2007.

[50] J. B. Anderson, *Digital Transmission Engineering*, John Wiley & Sons, Vol. 12. 2006.

[51] H. L. Van Trees, *Detection, Estimation, and Modulation Theory III*, John Wiley & Sons, 2001.

[52] A. N. D'Andrea, U. Mengali, and R. Reggiannini, "The modified Cramer-Rao bound and its application to synchronization problems," *IEEE Trans. Commun.*, vol. 42, no. 234, pp. 1391-1399, 1994.

[53] F. Gini, R. Reggiannini, and U. Mengali, "The modified Cramer-Rao bound in vector parameter estimation," *IEEE Trans. Commun.*, vol. 46, no. 1, pp. 52-60, 1998.

[54] F. Gini, and R. Reggiannini, "On the use of Cramer-Rao-like bounds in the presence of random nuisance parameters," *IEEE Trans. Commun.*, vol. 48, no. 12, pp. 2120-2126, 2000.

[55] D. H. Griffel, *Linear Algebra and Its Applications: A First Course v. 1 (Mathematics and its Applications)*, John Wiley & Sons, 1989.